PEOPLE'S DEMOCRATIC REPUBLIC OF ALGERIA

MINISTRY OF HIGHER EDUCATION AND SCIENTIFIC RESAERCH
AMAR TELIDJI UNIVERSITY - LAGHOUAT
FACULTY OF TECHNOLOGY
ELECTRONICS DEPARTEMENT

Promotion N° 11 / Univ. Lagh.
N° … / 2023 / Electronic

MEMOIRE

Dissertation Master Degreein Microelectronic Engineering
THEME

Numerical study and optimization of Thin film $Cu_2ZnSn(S_xSe_{1-x})_4$ absorbers For photovoltaic application using wxAMPS-1D

Presented by :
GRINAT Hicham

Before the jury composed of :

President :	Dr. M. BIRANE	University of Laghouat
Supervisor :	Dr. A. MOUHOUB	University of Laghouat
Examiner :	Dr. A. BELKHADER	University of Laghouat

2022/2023

Acknowledgments

We thank Almighty Allah for giving us the courage, will, health and patience to complete thiswork.

I would like to express my sincere gratitude to my supervisor, ***Dr. Abdelhafid Mouhoub****, fortheir invaluable guidance and support throughout my master's project. Their expertise and encouragement helped me to complete this research and write this project.*

I would also like to express my sincere appreciation to the members of the jury for their interest in my research and for agreeing to evaluate and enhance my work with their valuablesuggestions. Their contribution is highly valued and appreciated.

Furthermore, I would also like to thank my friends and family for their love and supportduring this process. Without them, this journey would not have been possible.

Finally, I would like to thank all of the participants in my study for their time and willingness to share their experiences. This work would not have been possible without their contribution.

Contents

Chapter I: Overview of principle physics of solar cells

Chapter II: Properties of CZTS compounds in thin layers and deposition processes

Chapter III: Numerical simulation and interpretation of results

General Introduction

General Introduction

Abundant availability and ecofriendly nature make renewables, the most viable alternate in all the energy sources. Although renewables were able to produce energy greater than the amount of energy they have used, issues like variability, intermittency, lack of technology for efficient energy storage, relatively high cost of raw materials etc., deterred the usage of the renewables in main stream energy production [1].

However, recent technological advancements, especially in solar energy sector such as the usage of new materials, reducing the influence of raw material price of absorbent layer on the overall cost of the cell and also recent fall in prices of raw materials have resulted in achievement of near grid parity [1].

Even though the materials like CIGS and CdTe appeared to be promising among the thin film solar cells with about 23% and 17% efficiencies respectively [2] , the use of less abundant materials such as indium and gallium are hard to extract which make them not an ideal choice for large scale grid level production. Also, Cd which is extensively used in the manufacture of active material is a toxic heavy metal and can be an environmental hazard. The materials such as kesterite–structured copper zinc tin Chalcogenide (Cu_2ZnSnS_4/Se_4) are recently considered as a potential replacement for CIGS and CdTe as they are made of earth abundant, inexpensive and non-toxic elements. Low band gap of the material ~1.0eV makes it a very good absorbent layer. Few champion cells have been built already with efficiency of around 10.1% [3].

$Cu_2ZnSn(S_xSe_{1-x})_4$ (CZTSSe) material is a promising candidate for low-cost and high efficiency thin film solar cells. Compared to other technologies CZTSSe offers the advantage of containing no critical chemical elements. This key aspect joined to its optical properties makes possible to foresee a photovoltaic thin film technology scalable at several GW/year [1].

The research of a trade-off between high performances and low processing cost CZTSSe has recently driven the attention of the scientific community. In order to become very interesting for production at industrial level, CZTSSe solar cell performances must be certainly improved.

The main objective of this work is to make a fairly in-depth study on the main factors likely to intervene to minimize the photovoltaic performance of the cells studied, and to optimize the photovoltaic parameters by studying the effect of the physical and electrical parameters as well as the composition chemistry of the absorber material in order to obtain maximum performance. . This explains and justifies the research concerning the study of

Digital design, modeling and simulation programs. To this objective, this work is approached according to the following chapters:

Chapter I was devoted to the study of the different photovoltaic parameters of importance in the manufacture of a solar cell. This chapter explains in depth the method of calculating the conversion efficiency of a solar cell.

Chapter II is intended for the study of absorber material based on CZTSSe compounds.

In the last chapter, we describe the different steps of the wxAMPS software, used in numerical simulation, and we give some numerical examples of simulation for different materials. The results thus obtained are commented on and interpreted thanks to the notions of the current voltage characteristic and the spectral response. Mastering the software and simulation techniques will allow us to study any region of the solar cell and all the physical parameters.

Finally, we finish our work with a general conclusion.

Chapter I:

Overview of principle physics of solar cells

I.1 Introduction

In this chapter we use some essential bases in the photovoltaic field, We will thus first approach some notions on the source of photovoltaic energy. We will then describe the semiconductors, the p-n junction and the solar cells with their photovoltaic characteristics and we end with a brief description of the different existing technological sectors.

I.2 The photovoltaic effect

The origin of the word "photovoltaic" is made up from the Greek word phos (light), and voltaic (electrical) from the name of Italian physicist Alessandro Volta. The physical basis for photovoltaics is the "photovoltaic effect". An appropriate definition of the photovoltaic effect is the direct conversion of light into electricity.

The term "solar cell" is employed to describe a device, which is able to convert the energy of the sun (light) into electrical energy.

The first observation of the photovoltaic effect (1839) is attributed to the French physicist Edmond Becquerel. He discovered that exposing to light two copper plates immersed in a solution, it is possible to produce a continuous flow of current. After that, an American engineer called Charles Fritts produced the first selenium-based solar cell (1883). However, the efficiency of Fritts cell was less than 1% which was not enough to justify it as a practical power source due to the cost of gold contacts.

1954 was the beginning of silicon technology for PV. It was discovered at Bell Labs that a silicon p-n junction could convert 6% of the incoming sunlight into electrical energy. In 1958, silicon solar panels were included on the American spacecraft Vanguard I. Hoffmann Electronics increased the efficiency to 14% and soon a market niche for silicon solar cells was discovered (1960). In the following 50 years, the global PV production has reached over 140 MW. The 21th century sees above all the ripeness of the thin film, dyesynthesized, and multijunction solar technology [4].

I.3 Current trends in PV technology

Renewable energy as photovoltaics is one of the alternatives to the *"conventional"* energy as nuclear, hydro, and coal. Nuclear has the 15% in world production of electricity. France, Japan, and USA depend on nuclear power plants (75%, 30%, and 19% respectively) in their whole energy resources [4]. A lot of countries, like Germany and Japan, are gradually switching to renewable energy as photovoltaics in order to reduce risk factor of nuclear energy. Total energy capacity of the world is 4742 GW in which the share of the solar

energy was 37 GW in 2010 (0.78%) [5]. In 2009, the new installation of solar energy was 97.1 GW that was more than doubled in 2010 (17.5 GW). The top 10 companies such as Qcells, Sharp, Suntech, Keyocera, First Solar, Motech, Solar World, Jasolar, Yingli, and Sanyo share the almost totality of the market.

Since its emergence thin film photovoltaics (TFPV) take on two difficult challenges:

I. to compete with silicon based PV in terms of power conversion efficiency and manufacturing costs,

II. to contain only earth-abundant and non-toxic materials without severe degradation in the long term. Moreover as long as crystalline silicon (c-Si) solar PV manufacturing costs decreases, TFPV solar cells will remain in the small minority.

In recent years, TFPV technology has experienced rapid growth and achieved significant technological advances, consolidating its place in the solar market. In 2012, TFPV represented approximately 10% of the global PV market (28.4 GW) [4]. From a physical point of view, the advantages of TF solar cells are to have a direct band gap, a high absorption coefficient which allow absorbing the majority of the solar spectrum using only few microns of materials, and reduced sensitivity to recombination at grain boundaries. Moreover, from a technological point of view, they either permit to decrease fabrication costs by exploiting manufacturing actions like roll-to-roll, or permit the usage of flexible substrates, and monolithic interconnections.

In thin film solar cells family, chalcogenide-based solar cells as $Cu(In,Ga)Se_2$, CdTe and $Cu_2ZnSn(S,Se)_4$ are the best candidates potentially reduce manufacturing cost of solar energy. Recently, First Solar Company proclaimed that the current cost of electricity by its CdTe solar panel is 0.70 $/W and aims to develop solar cells at the cost of 0.5 $/W [5].

I.4 Solar spectrum

Solar radiation is comparable to the one of a black body at 5800 °K [5]. Sunlight passes through the atmosphere, but scattering and absorption processes attenuate it. Solar irradiance spectrum occurs over a wide range of energies (or wavelengths). The Air Mass (*AM*) is the path length which light takes through the atmosphere, and is useful to quantify the reduction in the power of light when it is absorbed by the atmosphere. The Air Mass is defined as:

$$AM = 1/(\cos\theta) \qquad \text{(I.1)}$$

where θ is the angle from the vertical (zenith angle). When the sun is directly perpendicular to Earth surface, AM is 1. The standard spectrum at the Earth's surface is called AM1.5G, (the G stands for global): the AM1.5G spectrum (θ = 48.2°) has been normalized to give 1 kW/m^2. This spectrum is the normalized flux used to measure the performance of cells in laboratories. The standard spectrum outside the Earth's atmosphere is called AM0, because the light does not overcome the atmosphere barrier. This spectrum is typically used to predict the expected performance of cells in space. Both AM0 and AM1.5G spectra are compared in Figure I.1.

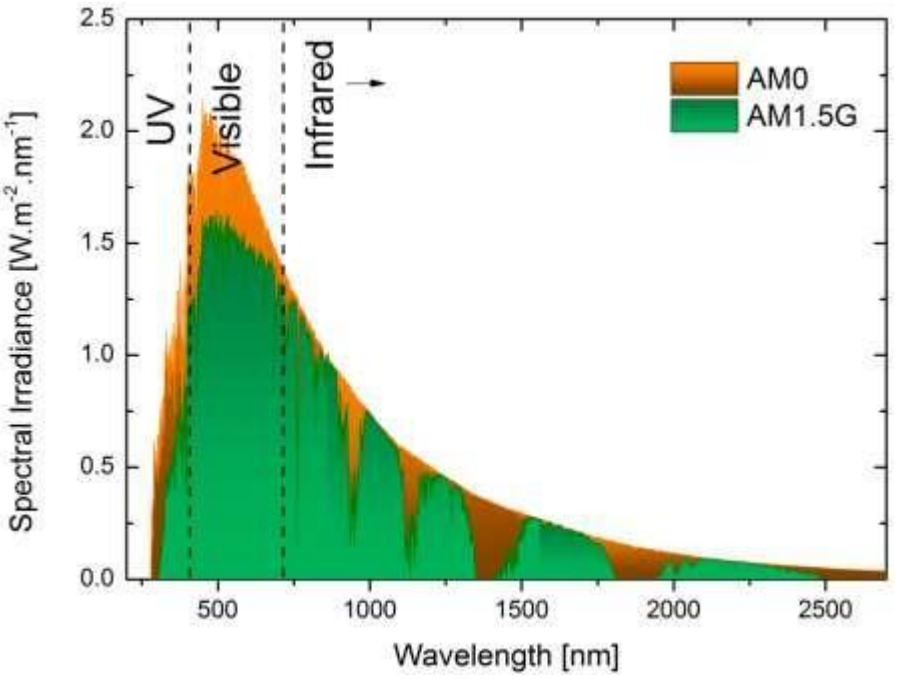

Figure I.1: Solar irradiance spectrum above atmosphere and at Earth surface [4].

I.5 Principle

Photovoltaics allow generating electrical power by converting solar radiation. Physics of photovoltaics is based on the optical and electrical properties of semiconductors. When a photon (hv) with energy higher than the bandgap of the semiconductor is absorbed, an electron-hole pair is created. This means that an electron is promoted from the valence band (E_v) to the conduction band (E_c) leaving a hole behind. This pair needs to be separated then by electric field in order to avoid recombination: this field is provided by a p-n junction which is the core of a photovoltaic device. A photon hitting on the surface of a semiconductor could be either reflected from the surface, absorbed in the material or transmitted throughout the material itself. In the case of PV devices, photons which are not absorbed (thus reflected or

transmitted) are typically considered as a loss since they do not generate power. Considering the energy of the photon and the bandgap of the semiconductor it is possible to establish if a photon is absorbed or transmitted :

- $E_{ph} < E_g$: photons with energy E_{ph} less than the band gap E_g are transmitted
- $E_{ph} = E_g$: photons with energy E_{ph} equal than the band gap are absorbed and can create an electron hole pair.
- $E_{ph} > E_g$: photons with energy higher than the band gap are also absorbed. However, for PV applications, part of the energy of these photons is released since electrons quickly thermalize down to the E_c lower energy states [6].

I.6 Junctions in semiconductors

There are three kinds of junctions in semiconductor devices: metal (schottky and ohmic) junction, homojunction and heterojunction semiconductors, all of which are used in solar cell devices. The metal-semiconductor junction is created at the interface, and it depends on the work function (the energy between Fermi level and vacuum level) for both the metal and the semiconductor [4].

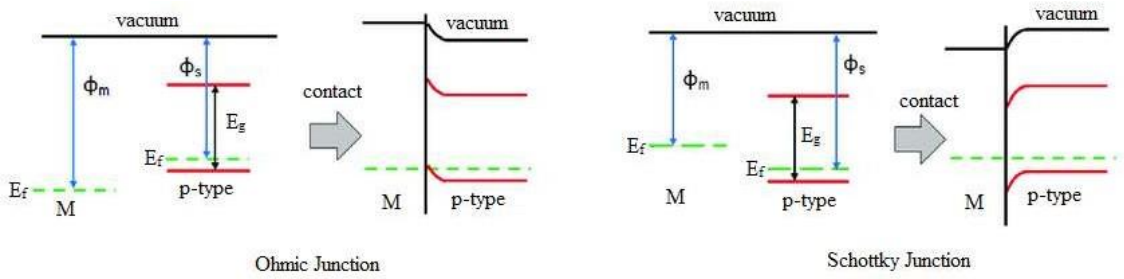

Figure I.2: Ohmic and Schottky junctions for a p-type semiconductor before and after contact.

Labels in the figure, M is metal, E_f is Fermi level, E_g is the energy bandgap, Φ_m is work function for metal and Φ_s is work function for semiconductor.

For the Schottky junction, when the metal comes into contact with the p-type semiconductor, the work function for metal is smaller than the work function of the semiconductor. Therefore, the holes diffuse to metal until the Fermi level is aligned, leaving behind the negatively charged acceptor atoms, and the depletion region is created in the semiconductor region. In this case, the hole will face a barrier height which is called the Schottky barrier, which prevents them from crossing the junction. For the Ohmic junction, it is created when

the work function of the metal is greater than the p-type semiconductor. Thus, the holes in the semiconductor will transport freely because they do not face any barrier as shown in Figure-I.3 [7]. The homojunction semiconductor is created when the p-type and n-type semiconductors are made from the same material, whereas the heterojunctions are created when they are made from different materials with different energy band gaps. However, in the heterojunction, a barrier to transport (energy spike) between p-n junction is created, whereas it does not appear in the homojunction.

I.6.1 Physics of p-n junction

In a doped semiconductor the more plentiful carriers are named "majority carriers", while the less abundant carriers are named "minority carriers". Majority carriers are electrons (holes) in n-type semiconductors (p-type semiconductors). Minority carriers are electrons (holes) in p-type semiconductors (n-type semiconductors). At equilibrium, the product of the majority and minority carrier concentration is a constant:

$$n_i^2 = n_0 . p_0 \quad \text{(I.2)}$$

Where n_i is the intrinsic carrier concentration, n_0 and p_0 are the electron and hole equilibrium carrier concentrations.

When an n-type and a p-type semiconductor are put in contact, a p-n junction is formed between the two materials. This event is the same in the case of homo-junctions or heterojunctions.

Once the two semiconductors are in contact, electrons from the n-region near the junction interface diffuse in the p-region leaving donor atoms electrically unshielded by the majority carriers. In the same way, holes from the p-region near the interface diffuse in the n-region, leaving acceptors unshielded behind. This phenomenon is called "diffusion". The region nearby the p–n interface, common at the two semiconductors, which lost its neutrality and become actively charged, is called the "space charge region" (SCR). The rest of the two semiconductors which is not influenced by the metallurgical junction is called "quasi-neutral region" (QNR). The consequence of the formation of the SCR is an electric field ($\bar{E}$) which fights the diffusion for both electrons and holes. $\bar{E}$ will superimpose on the random movement of carriers accelerating holes in the same direction of the field and electron in the opposite. This phenomenon is called "drift". When an equilibrium condition is reached, a potential difference (V_D) is formed across the p-n junction. The regions close to the junction become depleted of charge carriers, as shown in Figure I.3. This region is also called the space charge

region. The width of the depletion region depends on the built-in potential (which is a result of the differences between the Fermi energy levels of the p and n-types), the ionised acceptor N_A and the donor N_D concentration [6,7].

The built in voltage can be given by the difference between the Fermi levels of both p-type and n-type sides as a result of diffusion process:

$$= \frac{E_g}{q} + \frac{KT}{q} \log \left(\frac{NaNd}{N_c N_v}\right) \quad \text{(I.3)}$$

A schematic of the p-n junction is shown in figure I.3.

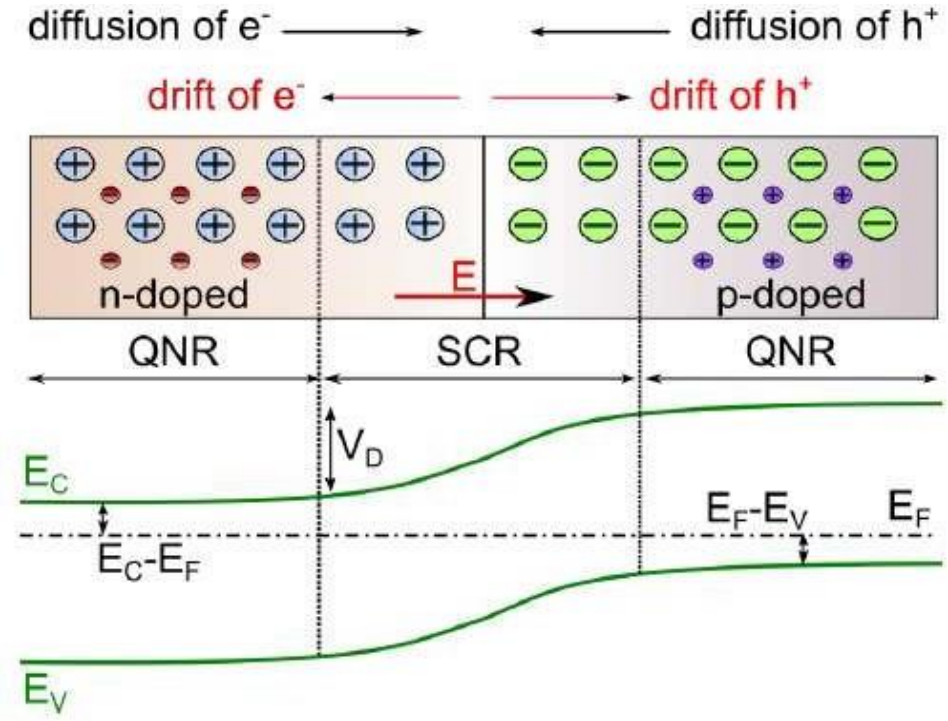

Figure I.3: p–n junction in thermal equilibrium with zero-bias voltage applied. Donor atoms (blue particles), acceptor atoms (green particles), electrons (red particles), holes (violet particles).

I.6.2 Current-voltage characteristics of a diode

The metallurgical junction introduced in the previous paragraph is the starting point to build a diode. In fact, the diode is a p-n junction connected to two contacts. It is possible to describe the diode current-voltage (*I-V*) characteristics (Figure I.4), though the following equation:

$$I = I(e^{\frac{g7}{nkT}} - 1) \quad \text{(I.4)}$$

Where I is the net current flowing through the diode, I_s is the dark saturation current, V is the applied voltage across the diode, n is the diode ideality factor, k is the Boltzmann constant, and T is the temperature.

I_s is defined as:

$$I_s = I_{00}(e^{\frac{gE_A}{nkT}} - 1) \quad \text{(I.5)}$$

I_s is the diode saturation current which is activated by the activation energy E_A and is the diode leakage current in the absence of light. E_A is the energy of the dominant recombination mechanism. I_{00} is called "reference current" which is only weakly temperature dependent. The n moderates the voltage dependence of the current density [6].

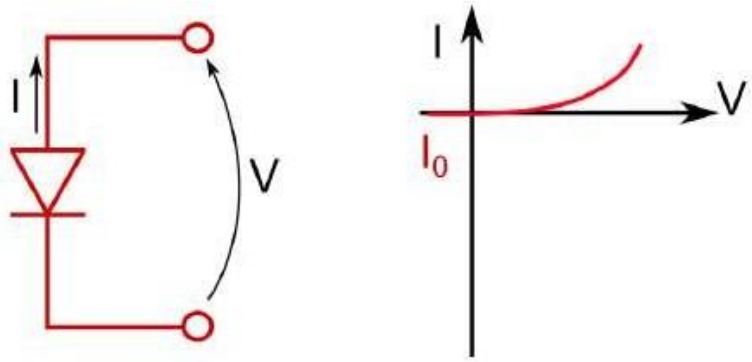

Figure I.4: Static I-V characteristics of a diode

I.6.3 Ideality factor

The ideality factor (n) is typically measured from the slope of the dark I-V characteristics. In ideal solar cell, the ideality factor is as much as possible close to one. Different magnitudes of n indicate that a specific recombination mechanism is dominant. Thus the variation of the ideality factor allows evaluating the type of recombination in solar cells.

I.7 Solar Cell Parameters

I.7.1 Light I-V characteristics

When a solar cell is illuminated under solar spectrum, additional electron-hole pairs are created giving rise to the so-called photogenerated current (I_{ph}) which could be model as a current generator in parallel to the diode. The I-V curve arises from the minority carrier properties which determine the solar cell behaviour. In general, the illumination shifts the J-V

curve of the p-n junction downwards in the current axis. The *I-V* equation of an ideal solar cell is given by:

$$I = I_{ph} - I(e^{\frac{g7}{nkT}} - 1) \quad \text{(I.6)}$$

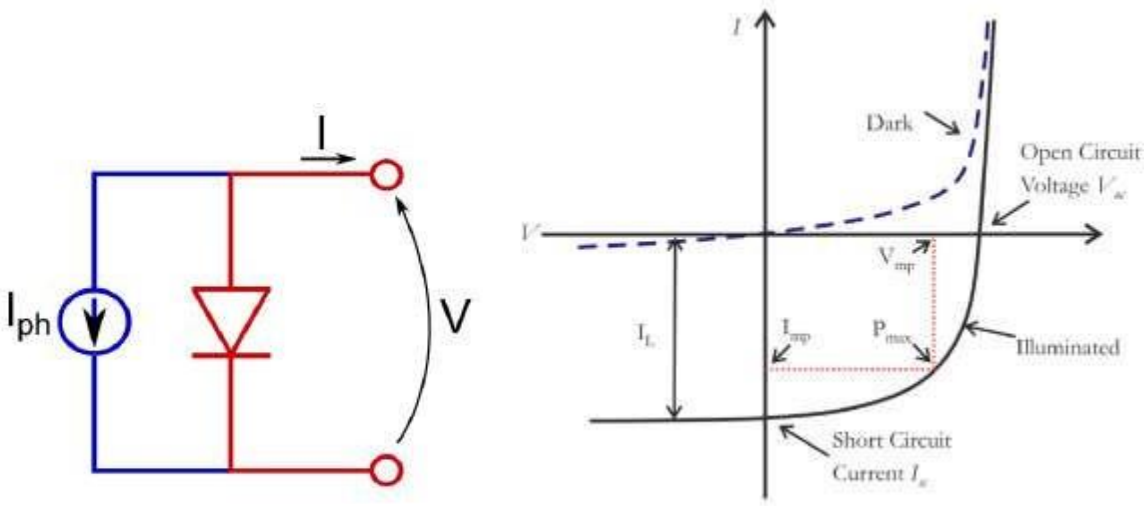

Figure I.5: Model and I-V curve of a solar cell under illumination.

I.7.2 Short-circuit current

The I_{sc} term in Figure I.5 is named short-circuit current defined as the current through the solar cell when the terminals are in short circuit (the voltage across the solar cell is zero). It is one of the figures of merit of a solar cell. By definition, I_{sc} is identical to $I_{ph}(0)$. The typical factors influencing *Isc* are the light intensity, the optical properties of the cell, the thickness of the p-n junction, and the collection probability [7].

I.7.3 Open-circuit voltage

Another figure of merit of solar cell is the so-called open-circuit voltage (V_{oc}): which is the voltage at the output of the cell when no load is connected. In this case the output current is zero ($I=0$), so the V_{oc} can be calculated from equation (I.6) as:

$$V_{oc} = \frac{nKT}{q} ln\left(\frac{I_{ph}}{Is} + 1\right) \approx \frac{nKT}{q} ln\left(\frac{I_{ph}}{I_s}\right) \quad \text{(I.7)}$$

I.7.4 Fill Factor

The fill factor (*FF*) is the third figure of merit introduced in this chapter. It is defined as the ratio between the square drawn by the values of the current (I_{MP}) and voltage (V_{MP}) of

the cell resulting in its maximum power point ($P_{MP}=V_{MP}\times I_{MP}$), and the square given by the product $V_{oc}\times I_{sc}$ (Figure I.6):

$$FF = \frac{PMP}{I_{sc}V_{oc}} \quad \text{(I.8)}$$

An ideal solar cell has a *FF* as closer as possible to one. In fact *FF* increases along with V_{MP} and I_{MP} approaching respectively V_{oc} and I_{sc}. To do that, it is mandatory to decrease the losses due to parasitic resistances inside the solar cell (parasitic resistance will be detailed further in the manuscript). Using this concept, it is possible to expose the *FF* as a measure of the losses of a solar cell.

I.7.5 Power Conversion Efficiency

The power conversion efficiency (*PCE*) is the most important figure of merit, which allows comparing solar cells each other. It is defined as the ratio between the generated electrical power (P_{MP}) and the solar energy (P_{IN}) to which the cell is exposed:

$$5 = PCE = \frac{P_{MP}}{P_{IN}} = \frac{I_{sc}.V_{co}.FF}{P_{IN}} \quad \text{(I.9)}$$

PCE depends on different parameters such as the intensity of the incident sunlight, the type of solar spectrum, the working temperature of the solar cell. For this reasons it is important, in order to compare the *I-V* characteristics of two or more devices, to carefully control the conditions under which *PCE* is measured. Typical measurement setup for terrestrial solar cells is with an AM1.5G spectrum at a temperature of 25°C.

I.7.6 External Quantum Efficiency (EQE)

EQE is a measure of how well a solar cell converts an incident photon into an electron and is defined as electrons generated divided by photons incident on the device. The measurement is performed by recording the current response of a solar cell to monochromatic light over a large range of wavelengths. It is defined by:

$$EQE(\lambda) = \frac{I_{ph}(\ )}{q(N)} \quad \text{(I.10)}$$

Where I_{ph} is the current generated by the light as a function of wavelength, N is the number of photons incident on the cell and q is the charge of an electron. It is useful because different parts of the *EQE* curve provide information about different loss mechanisms in the device. Figure I.6 shows an example of an *EQE* curve for a CIGS device (the device stack for this

technology is very similar to a CZTSSe stack). The numbers (1-6) correspond to the following loss mechanisms: [8,9]

1. Shading from the top grid.
2. Reflection from the front surface. Most high quality cells have an anti-reflection coating to minimize this.
3. Absorption in the top conducting electrode (ZnO).
4. Absorption in the bufer layer (CdS).
5. Incomplete absorption in the absorber (CIGS or CZTS).
6. Recombination in the device.

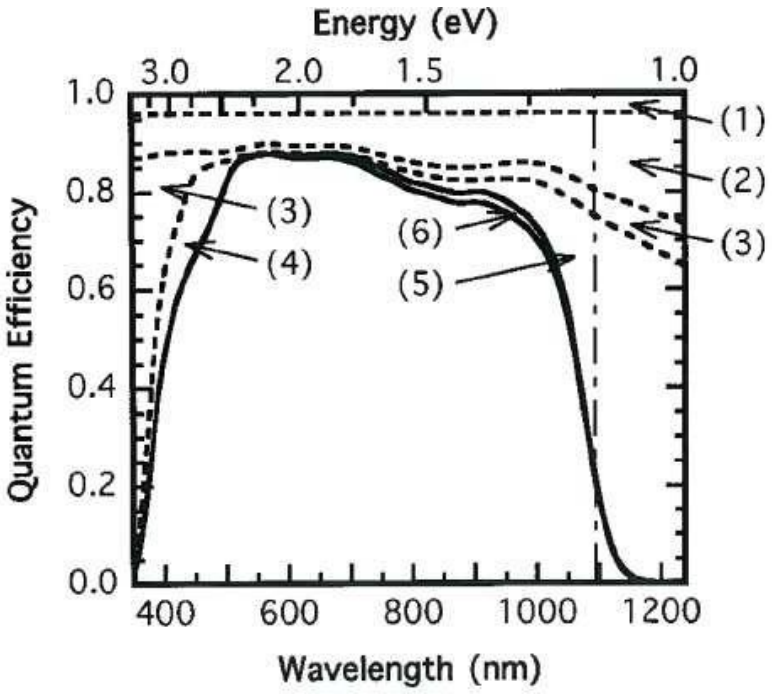

Figure I.6: Example *EQE* curve. The different loss mechanisms are marked and discussed in the text [6].

I.8 Losses in solar cells

Equation I.6 is considered for an ideal solar cell since it does not take into account series (R_s) and shunt resistances (R_{sh}) with are present into real solar cells. By incorporating these esistances in the model of Fig. I.7, what we obtain is equation 10:

$$I(V) = I_{ph} - I_s\left(e^{\frac{q(V+R_sI)}{KT}} - 1\right) - \frac{V+R_sI}{R_{sh}} \qquad (I.11)$$

The effects of these parasitic resistances are, in primis, to decrease the *FF* of the cells.

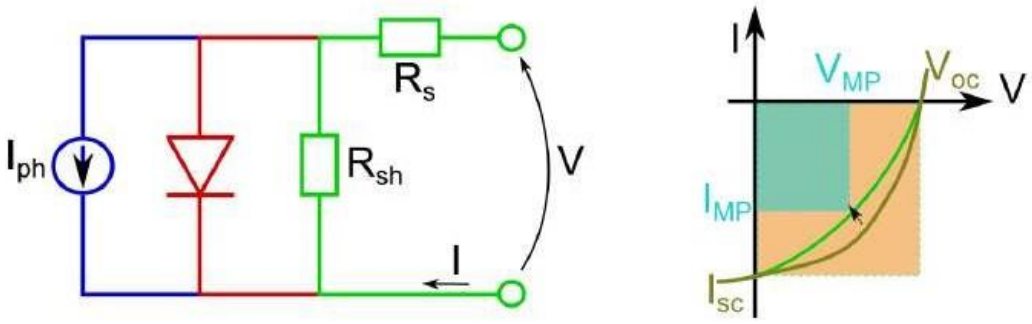

Figure I.7: Solar cell model including parasitic resistances.

I.8.1 Series Resistance

R_s variation is mainly affected by the resistances of the front and back contacts, and the resistance at the interface of the different layers [6,7]. High values of R_s may reduce the I_{sc}, contrary to V_{oc} where it has no effect (see Figure I.8).

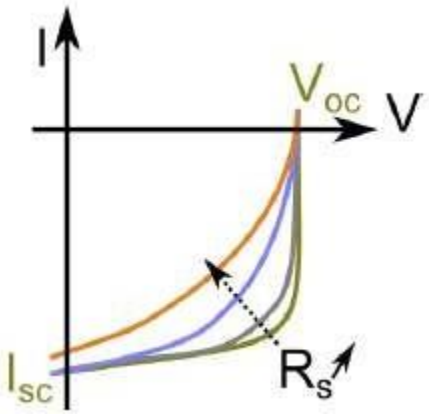

Figure I.8: Influence of R_s on photovoltaic characteristics under illumination.

I.8.2 Shunt Resistance

R_{sh} is a model of alternative paths (in particular short-circuits) for current. Its variations could be due to a non-perfect interface between the doped regions and the metal contacts, and to recombination in Shockley-Read-Hall (SRH) defects into the QNR. Contrary to R_s, R_{sh} must be as highest as possible in order to prevent lost in V_{oc} (see Figure I.9).

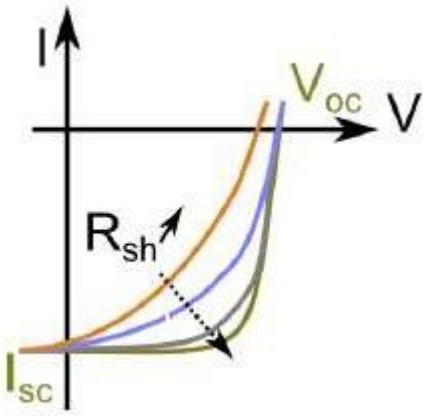

Figure I.9: Influence of Rsh on photovoltaic characteristics under illumination.

I.9 Solar cell

A solar cell is an opto-electronic device which, by photoelectric effect, directly converts sunlight into electricity. Its aim is to generate electric power. The core of a solar cell is the semiconductor p-n junction (see Figure I.10): once the sunlight is absorbed, an electron-hole pair is created and separated by the junction producing a current flow and a voltage across the contacts. Metal contacts at the edges of the p-n junction allow power dissipation when a load is directly connected (Figure I.10).

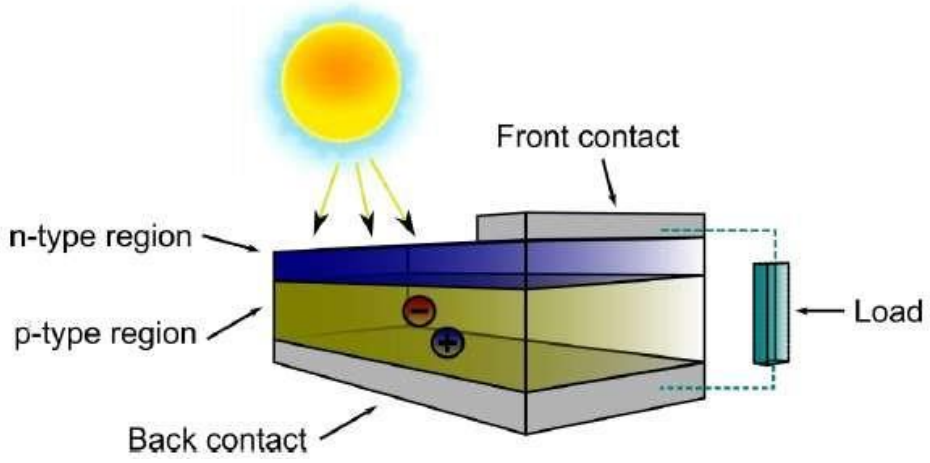

Figure I.10: Example of solar cell

I.10.1 Absorber materials of Solar Cells

There are many semiconductor materials that can be used in solar cell devices. In the following section, a brief explanation about alternative materials including silicon and thin film materials is presented.

I.10.1 Silicon Si

Silicon Si is the most popular solar cell material in the photovoltaic market. It has an indirect band gap of 1.1 eV, and it is used as a homojunction semiconductor device. It has been used widely for a long time, and extensive research on Si has been done to provide in depth knowledge about its properties and applications. Fabrication of silicon solar cells requires a high thickness (300-500 μm) , a pure crystal with more energy used of fabrication which leads to expensive solar cells [10]. There are three types of silicon used in the solar cell devices: single crystal, amorphous and polycrystalline. The single silicon crystal is recorded as having high efficiency in the range of 20 –25%. Amorphous silicon cells are thin-film solar cells, which are cheaper than the single crystal silicon. Also, their efficiency is lower than single crystals . The highest efficiency for amorphous silicon solar cells is in the range of 10–12% [10].

I.10.2 Gallium arsenide GaAs

It is one of the III-V semiconductor materials that have a direct band gap energy close to 1.43 eV and high absorption coefficient. It has many beneficial properties, such as low electronic effective mass, high-electron mobility, and high-saturation drift velocity, which make it ideal for optoelectronic and microelectronic devices like lasers, photovoltaic cells and light emitting diodes (LED). GaAs also has a zinc blende crystal structure. The highest conversion efficiency is 27.6 % [11]. The disadvantage of this material is its high cost, so it is used in the specific application such as satellites [11].

I.10.3 Cadmium telluride CdTe

CdTe is a p-type semiconductor with large absorption coefficient ($>10^4$ cm^{-1}) and a direct band gap of 1.45 eV. It has a zinc blende structure. CdTe devices are fabricated in the superstrate configuration with high conversion efficiency. First Solar, recently announced a new world record device efficiency of 22.1% [11]. Despite the progress made in CdTe technology by achieving cost-effective, high-efficiency devices, some issues connected with CdTe solar cells could affect their production in the future. The main issue is the toxicity and price of cadmium and relatively low abundance of tellurium, which could negatively impact production of CdTe thin film solar cells, leading to increased cell and module prices [12].

I.10.4 Chalcopyrite materials

Chalcopyrite is tetragonal crystal structure adopted by some semiconductors containing sulphur or other group VI elements along with group I and group III elements. Copper indium diselenide CIS is one chalcopyrite material with a direct band gap of 1.04 eV [13]. It is an alternative material for silicon and III-V materials and to improve the crystal quality and energy band gap, Ga was introduced , which leads to quaternary materials such as copper indium gallium diselenide (CIGS). CIGS has been the subject of extensive research and studies due to its structure and optical and electrical properties. It has a direct band gap in the range between 1.1 to 1.3 eV, which is close to the required value for optimum efficiency.The highest efficiency of CIGS is 22.9 % . The disadvantage of CIGS is that it has a rare and toxic elements including Ga and In [14].

I.10.5 Copper Zinc Tin Sulphide CZTS

This is an important material because it is low-cost and contains abundant elements compared with other thin materials. CZTS materials have a direct band gap of 1.5 eV with a high absorption coefficient of 10^4 cm^{-1}. It is a nontoxic material and is composed of elements abundant in the Earth's crust [35]. Moreover, copper, zinc, tin and sulphur are lower cost materials compared to indium and other common PV materials and it is similar to CIGS, though it replaces Ga and In [15]. The theoretical conversion efficiency limit is 32.2%, according to the Shockley and Queisser limit. The SQ limits for V_{oc}, J_{sc}, FF and efficiency are 1.3 V, 32 $mAcm^{-2}$, 87 % and 32% respectively [16,17].

I.11 Conclusion

In this chapter, we first presented solar radiation. Secondly we gave a reminder on semiconductors and the p-n junction, as well as the basic principle of operation of a photovoltaic cell and the exploitation of the current-voltage characteristic of the cell to calculate its various physical parameters. Finally we presented the different types of solar cells marketed.

Chapter II

Properties of CZTS compounds in thin layers and deposition processes

II.1 Introduction

From a technical point of view, today's commercially available thin film modules suffer from low efficiency like a-Si, shortage of raw material like Te in the case of CdTe, and In in the case of CIGS technology, or materials toxicity like Cd in CdTe technology. In this context, $Cu_2ZnSn(S_xSe_{1-x})_4$ (CZTSSe) appears to be a very attractive and highly potential material applied as a chalcogenide absorber in TF solar cells, regarding the fact that it is made from non-toxic (in the case of a pure sulfur-based compound, with no selenium), earth-abundant and low-cost raw materials, and shows high-efficiency potential for the near future [18].

This chapter will give an overview of the fundamental properties of $Cu_2ZnSn(S_xSe_{1-x})_4$, namely its crystalline structure, its electrical and optical properties, as well as the various experimental methods most in demand for the development of this thin-film material.

II.2 Material properties

In the last ten years, numerous investigation at theoretical level, have been carried out in order to predict the formation mechanism and the physical properties of CZTSSe compounds. The formation of I_2–II–IV–VI_4 compounds like CZTSSe can be achieved from an II–VI semiconductor by sequential replacement of cations in which the octet rule is respected and the total charge remains neutral (see Figure II.1).

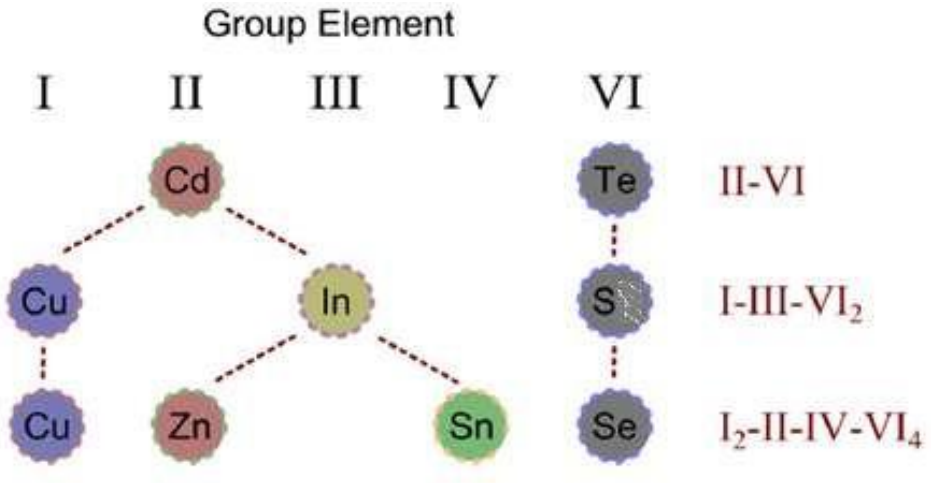

Figure II.1: Formation of stoichiometric I2–II–IV–VI4 compounds can be achieved by a sequential replacement of cations [11].

II.2.1 CZTSSe crystal structure

Binary compounds like CdTe adopt the cubic zincblende structure in which there are two interpenetrating face-centered cubic crystals [19]. The ternary I–III–VI_2 semiconductor alloys like CIS (in this case a chalcopyrite structure) can be built by replacing the group II atom with two atoms of group I and III [11]. Always respecting the octet rule, it is possible to split the ternary I–III–VI_2 compound by replacing two atoms of group III with two atoms respectively from group II and IV, forming a I_2–II–IV–VI_4 semiconductors. Composition of quaternary compounds in a phase diagram can be rather complex to display. Since each element can in principle be varied independently of the others, we have to be very careful when using terms such as 'Cu-poor', 'Zn-rich' etc., which are commonly employed to describe CZTSSe films. These terms are intelligible when only one component varies, but when two or more components deviate from stoichiometry, the terminology can be misleading.

The fact that the chalcogens (S, Se) are not an independent variables, allows representing the alloy in a ternary phase diagram. In fact the amount of anions (chalcogens) introduced in the alloy depends on the amount of the cations and their valency: Cu(I), Sn(IV) and Zn(II). In the CZTSSe literature, the ratios of atomic percentages [Cu]/([Zn]+[Sn]) and [Zn]/[Sn] are often used to represent the composition of the cations in the alloy. Both ratios are equal to one when the material is stoichiometric. However, these ratios are not independent, and therefore do not clearly show the deviations from stoichiometry in a particular case. A ternary phase diagram is the most useful way to summarize compositions in the Cu-Zn-Sn system. An example of a ternary phase diagram is shown in Figure II.2 [11].

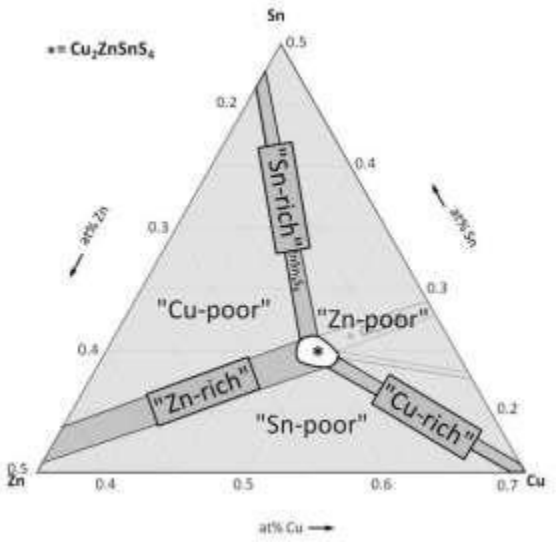

Figure II.2: Ternary composition diagram showing the position of stoichiometric CZTSSe [11].

One property of CZTSSe material is the possible shift from its stoichiometric composition leading in particular to Cu-poor compounds. The latter phenomenon originates from the inclination of the hosting crystal to stabilize copper vacancies, in which the charge balance is commonly insured by appropriate substitutions on the cationic sites.

CZTSSe crystallizes in a structure which could be kesterite (space group) [8,20], stannite. The stannite structure differs from that of the kesterite by the stacking sequence of the cations layers along the c-axis, i.e. (…–[ZnSn]–[Cu_2]–[ZnSn]–[Cu_2]–…) for stannite versus (…–[CuSn]–[CuZn]–[CuSn]–[CuZn]–…) for kesterite.

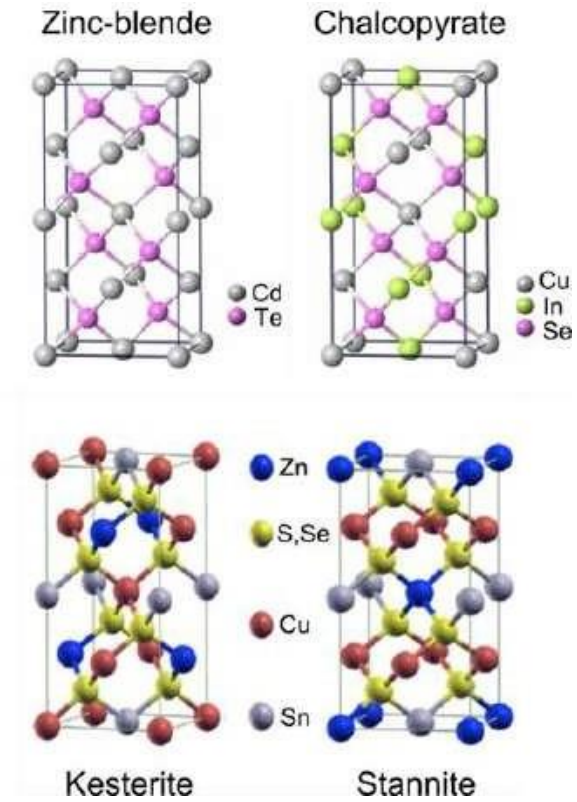

Figure II.3: Crystal structure representation of binary, ternary and quaternary compounds [11].

In the case of kesterite, it is also possible to have a so called disordered kesterite in which a random on-site distribution of Cu and Zn (50/50) occurs in the Cu/Zn layer leading to a higher symmetry [2]. Lafond *et al.* report that disordered-kesterite and kesterite models are still open to debate since they are very similar (Figure II.2) and almost undistinguishable [14]. The only differences lye in the splitting for symmetry reasons of the 4d position into 2c and 2d positions (Wyckoff notation) going from a slight change in the position chalcogens anions. It is recurring to have kesterite and stannite structure in the material at the same time due to a

low energy difference (~3 meV per atom) in which the cations (Cu, Zn, Sn) are fixed, and the anions (S, Se) are randomly distributed [14]. This energy difference could undergo also a bandgap variation of the material of 0.15 eV between kesterite (lower value) and stannite (higher value) . Details about the different crystal structures are shown in Figure II.3. Since the kesterite phase is the more likely to have (more stable) for CZTSSe material, only this one will be taken as reference in the rest of the manuscript (Figure 17). Lafond *et al.* and his group at Nantes University demonstrated:

i. a deviation in composition between the surface and the bulk for non-stoichiometric Cu-poor and Cu-rich CZTS using EDX and X-ray photoelectron spectroscopy [21],
ii. the ability of the CZTS phase to tolerate substitutions, i.e. deviations of the Cu2ZnSnS4 stoichiometric composition, without collapse of the structure and maintaining the overall charge balance in a proved Cudeficiency range ([Cu]/[Zn+Sn]) between 0.79–1.14 [14].

II.2.2 CZTS vs. CZTSe vs. CZTSSe

CZTSSe is a compound formed by mixing pure sulfide CZTS and pure selenide CZTSe materials. While these two materials have some differences, they have very similar optical and electronic properties and the same crystal structure. [9] Furthermore, when the two compounds are mixed to create a hybrid sulfo-selenide material, it has been reported that the crystal structure is retained through the entire range of sulfur to selenium ratios [22,23]. Figure II.3 shows the crystal structure for these materials. The grey atoms are copper, black atoms zinc, blue atoms tin and red atoms can be either sulfur or selenium.

II.2.3 CZTSSe bandgap

The chalcogens concentration into CZTSSe alloys gives the possibility to make band engineering to tailor the material properties for a given application, but at the same time, allows having some alloy disorder. Calculations of the electronic band alignment of $Cu_2ZnSn(S_xSe_{1-x})_4$ alloys by density functional theory (DFT) reveal a direct bandgap monotonically increasing from 1.0 eV (pure CZTSe) to 1.5 eV (pure CZTS) [19,20] with a small bowing parameter ($b \sim 0.1$) as reported in equation 11.

✓ $E_g(x) = (1-x)E_g(CZTSe) + x\,E_g(CZTS) - bx(1-x)$, (IV.1)

Since *b* is small, it is possible to approximate as linear the *EG* variations as a function of *x*.

The bandgaps decrease with increasing Se content, as shown in Fig. II.4. But they are not controlled linearly, which may be caused by the different absorption characteristics of nanoparticles with different sizes and morphologies.

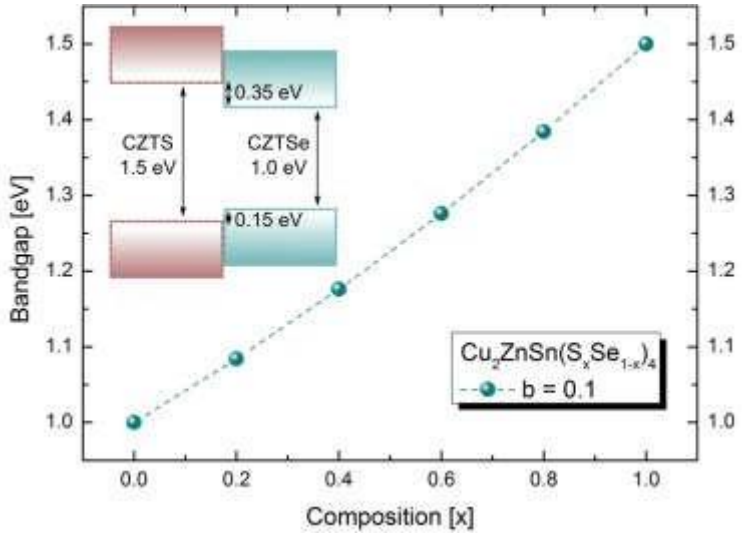

Figure II.4: $Cu_2ZnSn(S_xSe_{1-x})_4$ bandgap variation as function of the composition (x). In the inset the Type I band alignment between CZTS and CZTSe [24]

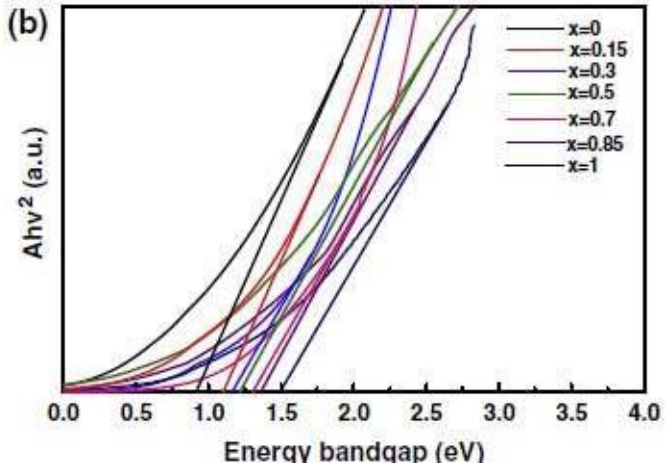

Figure II.5 An extrapolation of the spectra to identify the band edge of $Cu_2ZnSn(S_xSe_{1-x})_4$ nanoparticles [24]

II.2.4 CZTSSe absorption coefficient

CZTSSe material owns an optical absorption coefficient higher than 10^4 cm^{-1} at wavelengths lower than the band gap measured by absorption spectroscopy [24]. This permits to absorb light with an absorber of very thin thickness (1-2 μm).

Figure II.6 shows the UV–Vis absorption spectra of $Cu_2ZnSn(SxSe_{1-x})_4$ films dispersed in chloroform. All the $Cu_2ZnSn(S_xSe_{1-x})_4$ films demonstrate the well absorption features in the

visible light range. The absorption coefficient A is related to the incident photon energy hν as:

$(Ahv/K)^2 = hv - E_g$

Where K is a constant, and E_g is the optical bandgap [25].

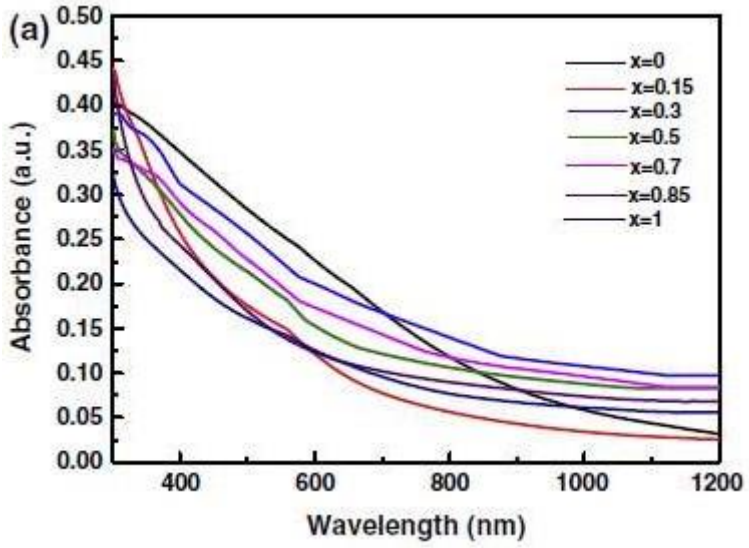

Figure II.6: UV–Vis absorption spectrum of $Cu_2ZnSn(S_xSe_{1-x})_4$ thin films with different x values [24]:

II.3 CZTSSe defects and doping

Due to higher number of constituent atoms compared to binary or ternary compounds, CZTSSe has a wider range of possible defects depending on its growth conditions and variations from stoichiometry [18, 30-32]. Most of them are antisites, vacancies, or interstitials: they can be located shallow or deep in the bandgap, and their concentration depends on their own formation energy [26]. In particular, shallow level defects can influence the minority and majority carrier concentrations thus the conductivity, whereas deep level defects may act as recombination centers for photogenerated electron-hole pairs. The most familiar defects, with their formation energies as function of the position within the bandgap, for pure CZTS and CZTSe are summarized in Figure 19. The two graphs in Figure 19 could explain why the p-type conductivity of CZTSSe is mainly due to the antisite Cu_{Zn}: its formation energy is lower than all the others acceptors defects (V_{Cu}, V_{Zn},Zn_{Sn}, Cu_{Sn}) although they can be present in the alloy [26]. From this analysis it is possible to explain the reason of the higher efficiency for Cu-poor and Zn-rich CZTSSe solar cells [27]: indeed this composition allows the increase of shallow Cu vacancies in spite of Cu_{Zn} antisite. Moreover, the high formation energy of donor defects (Sn_{Cu}, Sn_{Zn}, Zn_{Cu}, Cu_i, Zn_i), explains why n-type doping of CZTSSe is very difficult.

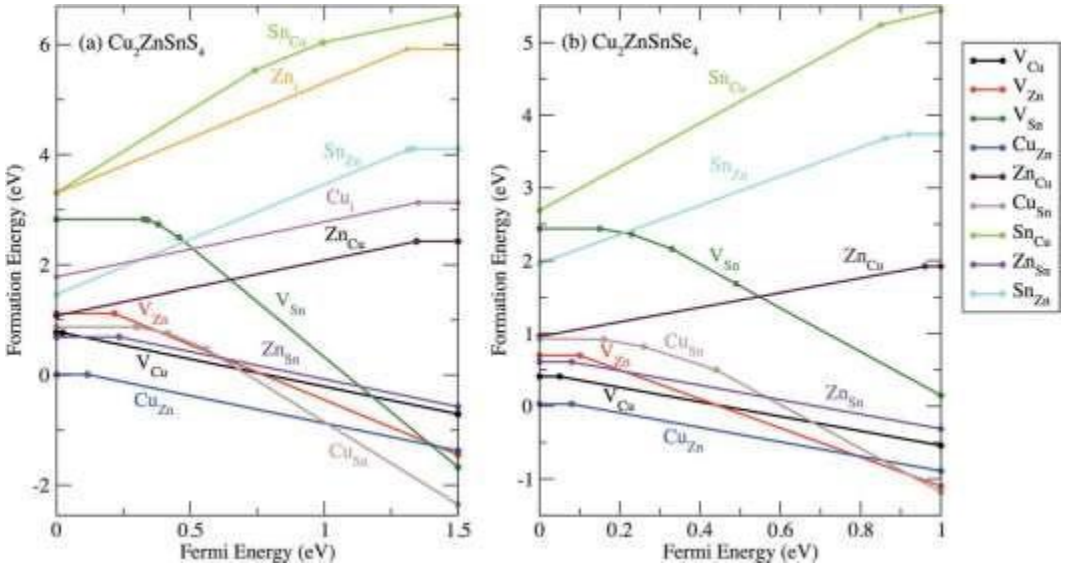

Figure II.7: Calculated defect formation energy as a function of the Fermi energy for a Cu-poor and Zn-rich CZTSSe [4],

The more CZTSSe is non-stoichiometric the more deep levels caused by the intrinsic defects increase [16, 30, 34]: some of them may act as traps for free carriers, which reduces the efficiency of solar-cell devices [26]. Chen *et al.* presume that chargecompensated defect complexes are easy to form in CZTSSe. They may passivate the deep donor levels improving CZTSSe quality and thus solar cell efficiency [27]. In particular the formation of the $[V_{Cu}^{-} Zn_{Cu}^{+}]^{0}$ cluster under Zn-rich and Cu-poor conditions is predicted to be beneficial for CZTSSe solar cell performance; however, the precipitation of a ZnS phase must be avoided [4,27].

II.4 Technological $Cu_2ZnSn(S,Se)_4$ synthesis

Different techniques, vacuum or non-vacuum, are employed to synthesize CZTSSe absorber.

II.4.1 Vacuum techniques

One-step vacuum processes consist in simultaneously incorporating all the elements. Among these techniques employed for high-quality CZTSSe deposition, co-sputtering [11] and co-evaporation [28] can give good PV performances. Other interesting methods can be pulsed-laser deposition [29]. The so-called two-step process is a technique where the precursors are first incorporated during an ambient temperature process like sputtering or evaporation, followed by an annealing step. The chalcogens can be incorporated into the precursor or during the annealing step. The annealing step could be a selenization or sulphurization process [11].

II.4.2 Non-vacuum techniques

Non-vacuum deposition methods for CZTSSe synthesis, as well as for other applications, are scalable and low-cost processes with the goal of being attractive for large scale manufacturing. The world record efficiency for CZTSSe solar cell (12.6 %) has been achieved following one of these approaches: the simultaneous use of spin-coating solution and particles of constituents [11]. Other possible methods giving a quite good PV performance CZTSSe could be nanoparticles [30] and electroplating [31]. One weak point of these techniques is, in some cases, the use of toxic and dangerously instable solvents which are hard of recycling as hydrazine.

II.5 Device Fabrication

The standard device stack used for CZTSSe comes directly from the CIGS stack developed at the National Renewable Energy Laboratory (NREL). [32] Figure II.8 shows the di↵erent layers in this stack, which starts with a soda lime glass substrate. A molybdenum layer is then sputtered onto the glass as the back electrode. This layer is followed by the absorber (CZTSSe/CIGS) and the CdS buffer layer. The purpose of the buffer layer is to complete the p-n junction and protect the absorber from damage during deposition of subsequent layers. The next layer is a thin i:ZnO layer deposited to increase the shunt resistance of the devices and is followed by a transparent conductive top electrode. While the best CZTSSe devices are made using this device stack, it is unlikely that it is ideal for CZTSSe since it was originally developed for a different material.

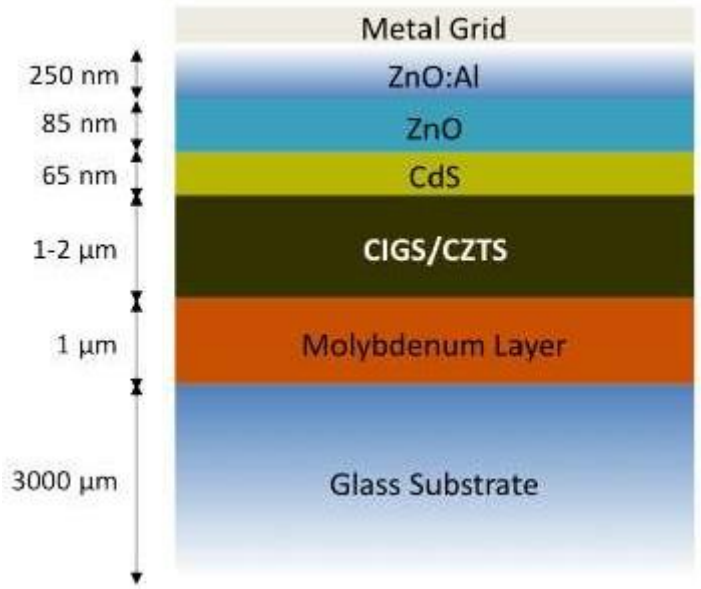

Figure II.8: The CIGS device stack that has been adapted for CZTS.

A testable device was prepared by incorporating CZTSSe films into the well established CIGS device stack described in section 2.5.5. The molybdenum layer was either deposited in chamber #1 or bought from UHV Sputtering Inc. (the stress state of this layer was not controlled). After CZTSSe deposition, a 65nm CdS film was deposited using the Chemical Bath Deposition (CBD) method developed at NREL. [33] To increase shunt resistance, a 85nm i:ZnO layer was deposited using RF sputtering and a conductive 250nm Al:ZnO layer was deposited using DC sputtering to act as a top electrode. A metal grid was screen printed onto the Al:ZnO to minimize series resistance further.

II.6 Conclusion

In this chapter, we have described some fundamental structural, electrical and optical properties of p-type CZTSSe compounds which constitute the essential part for the photovoltaic cell (the absorber layer). Then we ended this presentation with the process of depositing thin layers of the CZTSSe absorber which is also an opportunity to reduce costs. Currently dominated by vacuum deposition such as cathode sputtering or co-evaporation, the fabrication of photovoltaic modules by the non-vacuum route is a tremendous opportunity to reduce equipment investment costs, reduce precursor losses and increase production rates.

Chapter III:

Numerical simulation and interpretation of results

III.1 Introduction

Recently, because of the high costs of experimentation (technical development and characterization), the researchers turned to simulation [35]. Numerical simulation has become essential for all areas of research and especially for electronic or optoelectronic components and in particular in photovoltaic cells. This simulation software gives us the possibility to study and interpret the results obtained, in order to optimize the structure and the various cell components to improve their performance. Among the software available, our choice is for the wxAMPS-1D.

In this chapter, we present the study of the electrical characteristics of the heterojunction solar cell (n-ZnO/n-In_2Se_3/p-CZTSSe) in thin layers. Where the semiconductor p- $Cu_2ZnSn(S_xSe_{1-x})_4$ (CZTSSe) which is the absorber of the cell. We studied the influence of the different parameters for each layer of the cell in order to improve the conversion efficiency η(%), the short-circuit current density I_{sc}, the voltage in open circuit V_{oc} and form factor *FF*. We will recover all this from the WxAMPS-1D simulator to generate the results of the electrical characteristics of the studied cell and their talks.

III.2. Presentation of the wxAMPS-1D simulation software

III.2.1. Insight

AMPS-1D (Analysis of Microelectronic and Photonic Structures in one Dimension) [35,36] is one of the most chosen simulation software for analysis and design of transport phenomena in microelectronics and in structures photonics This software was developed in 1997 by Professor Stephen Fonashet et al. [35]. This is a single dimension that is applicable to any two-way device terminals. It can be for diode, photodiode sensor and device analysis photovoltaic [36].

wxAMPS is an update of the popular solar cell simulation tool AMPS, it is a numerical simulation software for one-dimensional solar cells, designed at the University of Illinois at Urbana Champaign, in conjunction with the University of Nankai in China [35]. The wxAMPS user interface uses a cross-platform library and allows fast data entry and improved visualization. Beyond the AMPS Core wxAMPS incorporates two tunneling models and a new algorithm combining the methods of Newton and Gummel. The incorporation of a tunnel model trap-assisted allows more accurate simulation of multi-junction solar cells. The combined solutions of the methods of Newton and Gummel improve the code stability and

allow both tunneling models to work well in the algorithm. Based on the option of an unlimited number of layers in the simulation, the modeling of dimmed solar cells can be easily implemented in wxAMPS [35].

III 2.2 Description of the wxAMPS model

In the electric model, three associated differential equations: the equation of Poisson and the two charge carrier continuity equations are solved simultaneously in the equilibrium state and out of thermodynamic equilibrium (i.e. under the effect of bias voltage or light, or both). The continuity equations governing the condition of dynamic carrier equilibrium in the semiconductor. They are written, in one dimension:

III.2.2.1 Continuity equation

The continuity equations govern the dynamic equilibrium condition of the carriers in the semiconductor. They are written, in one dimension:

$$\frac{\partial n}{\partial t} = n\mu_n \frac{\partial E}{\partial x} + \mu_n E \frac{\partial n}{\partial x} + D_n \frac{\partial^2 n}{\partial x^2} + g_n - \frac{n - n_0}{\tau_n} \quad \text{(III.1)}$$

$$\frac{\partial p}{\partial t} = -p\mu_p \frac{\partial E}{\partial x} - \mu_p E \frac{\partial p}{\partial x} + D_p \frac{\partial^2 p}{\partial x^2} + g_p - \frac{p - p_0}{\tau_p} \quad \text{(III.2)}$$

III.2.2-1 Poisson equation

Any space charge ρ(x,y,z) is accompanied by an electric field given by Gauss's theorem:

$$\vec{\nabla}.\vec{E} = \frac{\rho(x, y, z)}{\varepsilon} \quad \text{(III.3)}$$

where ε is the dielectric constant of the semiconductor. The electric field is on the other hand connected to the potential by the relation , which gives by explaining in the expression (III.3).

$$\nabla^2 V = -\frac{\rho(x, y, z)}{\varepsilon} \quad \text{(III.4)}$$

This is the Poisson equation, the integration of which makes it possible to calculate the variation of the potential in a semiconductor from the space charge. The space charge is calculated by taking into account all the charges that exist at a point of the semiconductor, i.e.

on the one hand the mobile charges which are the electrons and the holes, and on the other hand the fixed charges which can be localized on ionized donors or acceptors or on deep centers. In the absence of deep ionized centers, this space charge is given by:

$$\rho = e\left(N_d^+ - N_a^- + p - n\right) \quad \text{(III.5)}$$

III.3 Description of wxAMPS interface

The wxAMPS interface (Figure III.1) consists of three dialog boxes. Each gives the necessary parameters before launching the simulation by the wxAMPS. The three dialog boxes give:

- Environmental conditions;
- The material properties of each layer;
- Modeling parameters.

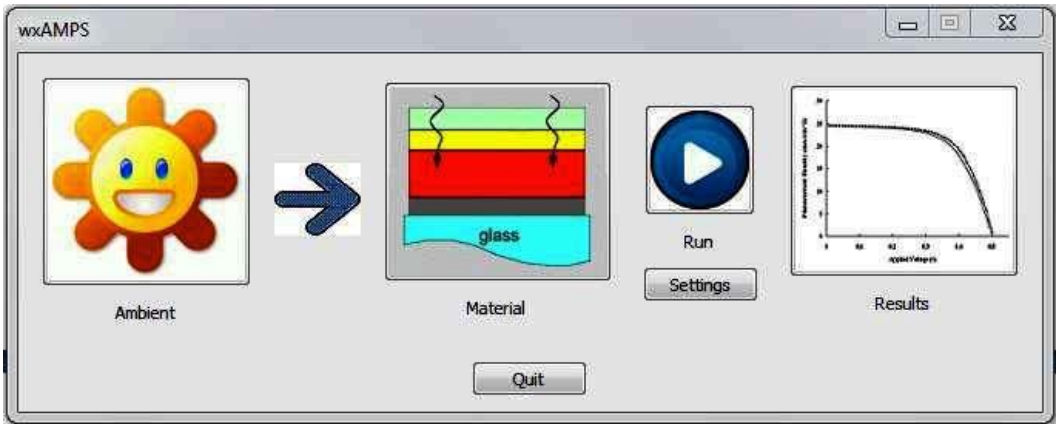

Figure III.1: User interface home page.

III.3.1 Environmental conditions

The environmental conditions interface (AmbientDlg) in the wxAMPS software is shown in the figure (III.2), we enter the parameters as temperature, the light spectrum file, the *QE* quantum efficiency file and the "Bias" file voltages" in the dialog box [35,36].

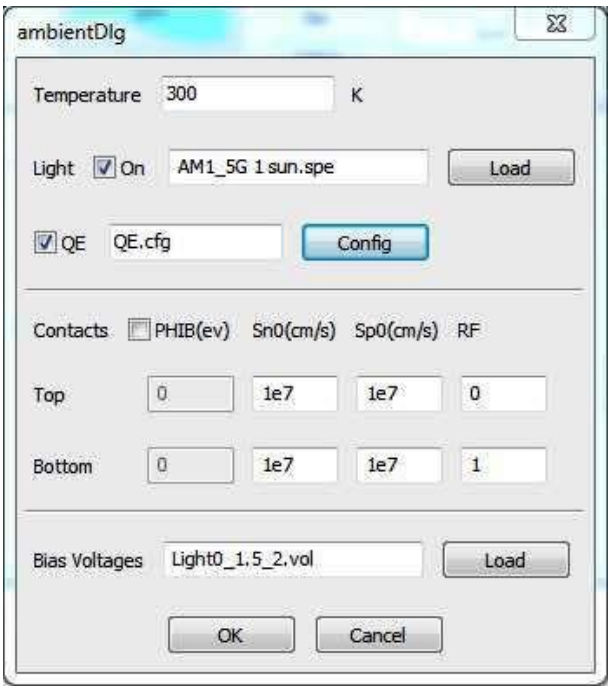

Figure III.2: The environmental conditions interface.

III.3.2 Material properties of each layer

The material properties interface of each layer (MaterialDlg) is represented in the figure (III.3):

- ✓ The layers and their thicknesses: they are represented in the figure
- ✓ The electrical properties of each layer such as permittivity, gap energy (E_g), affinity, mobility, Density of effective N_C, Density of effective N_V …as shown in figure (III.3).
- ✓ The defect parameters (capture cross sections, densities, level of energy), they are represented in the figure (III.4).
- ✓ The optical properties (absorption coefficient) of each layer. they are represented in the figure (III.5).
- ✓ Advanced parameters (numerical convergence parameters): they are represented in the figure (III.6).

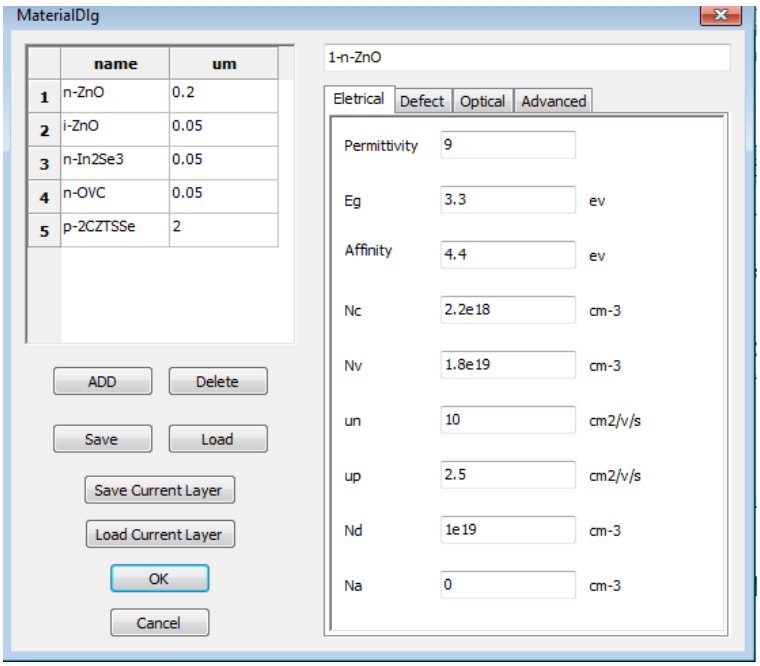

Figure III.3: The material properties interface of each layer.

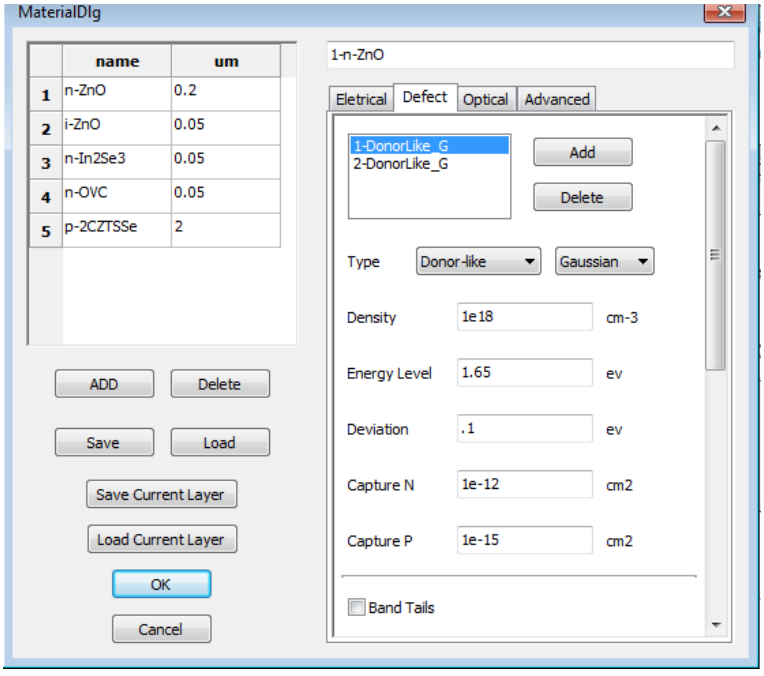

Figure III.4: The material properties interface of each layer (Defect).

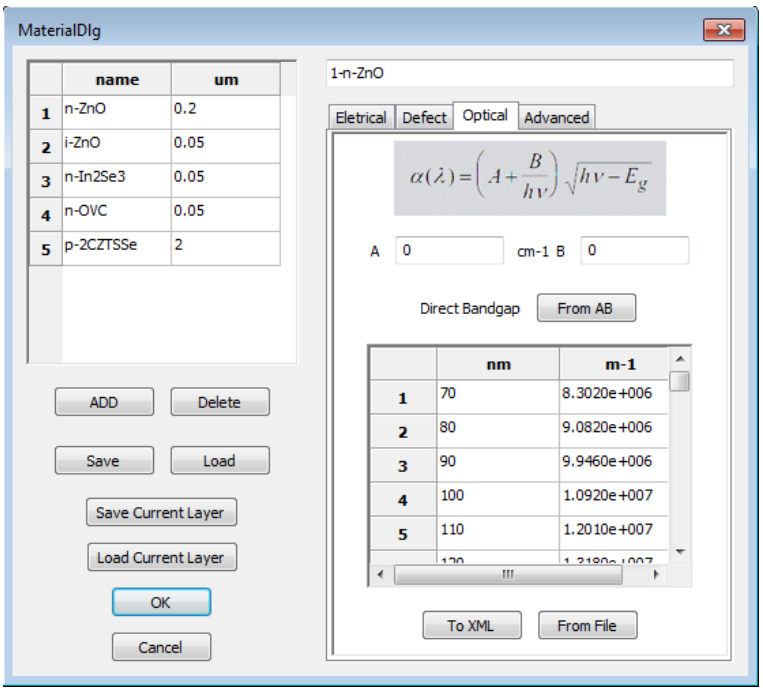

Figure III.5: The material properties interface of each layer (Optical).

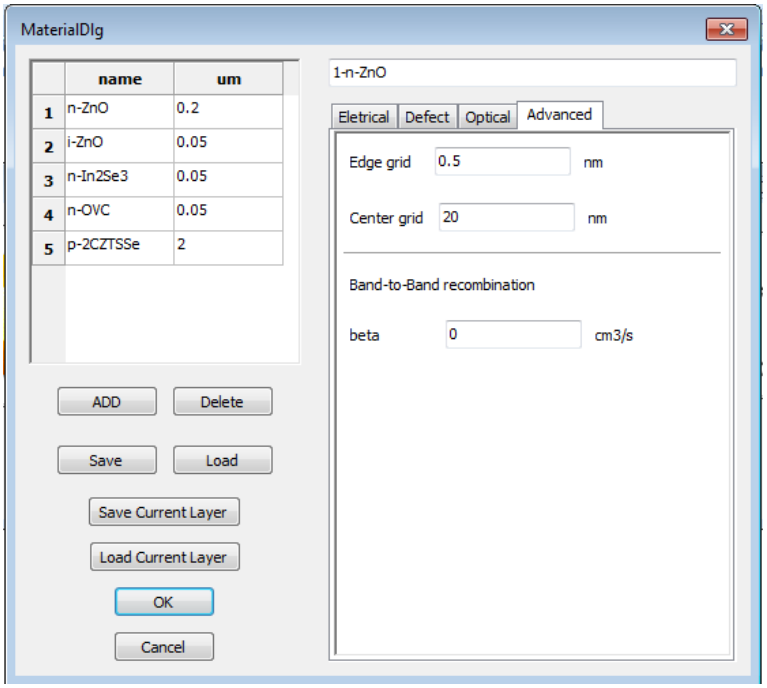

Figure III.6: The material properties interface of each layer (Advanced).

III.3.3 Modeling parameters

To modify the modeling parameters, we press on the "Settings" mode at the software interface (figure III.7)

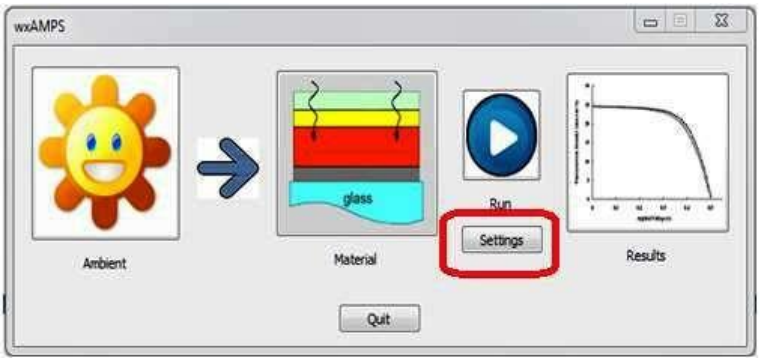

Figure III.7: The wxAMPS interface (Settings).

A new window opens, we make changes to it (see figure III.8).

- The type of the model:
  - Trap-assisted Tunneling.
  - Intra-band Tunneling.
- Numerical parameters:
  - Iteration Times Limit;
  - Converging Precision;
  - Clamping Range.
- TAT Setting:
  - Improved mobility (Mobility Enhanced).

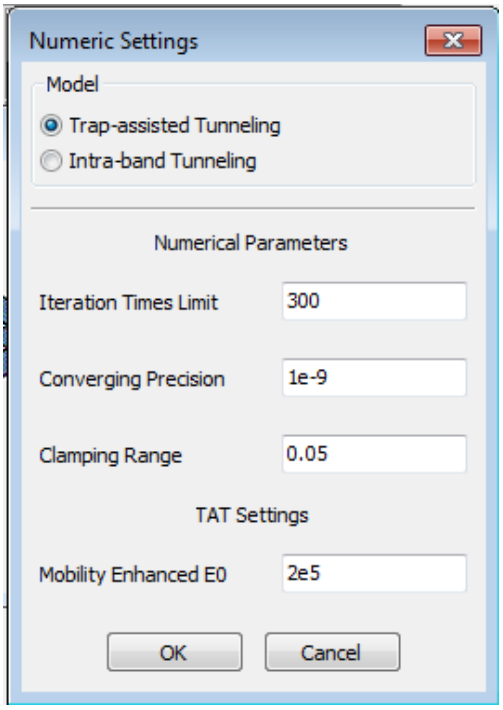

Figure III.8: The modeling parameters interface.

For the simulation, we tick the "OK" box and so the software starts execution (Figure III.9). During the simulation process, a dialog box progress is displayed, which lets users know that the calculation is complete normally (Figure III.10).

Figure III.9: Dialog box for The execution interface.

Figure III.10: Dialog box for progress is displayed.

When the calculation is finished, the results are stored and presented by curves as shown in figure (III.10). They are the characteristics (*J-V*) in the dark and under illumination, the values of the saturation current density (J_s), of the factor ideality (*A*), parallel resistance (shunt) R_{sh} , series resistance R_s , density short-circuit current (J_{sc}), open-circuit voltage (V_{oc}), factor fille (FF), photovoltaic conversion efficiency, quantum efficiency external (*QE*) as well as the internal quantities such as the diagram of the energy gap, the densities of free or trapped carriers, the electric field and potential, the rate of recombination, the current components of electrons and holes, the durations of life…etc [38,39].

III.4 Device structure and simulation

The CZTSSe cell structure is composed of the following layers of material: n-ZnO:Al, i-ZnO, n-In_2Se_3, p- CZTSSe absorber, p^{++} CZTS and Mo on glass substrate. A thin surface layer, which is designated as an OVC, is present between the CZTSSe and In_2Se_3 layers. The simulation program WxAMPS-1D was used in this study. For the simulation properties of the cell structures of the CZTSSe. Several parameters can be calculated by this program in dark and under illumination. It includes the quantum efficiency, the current-voltage (*J–V*)

characteristics, the electric field, the reflectivity, the free and trapped carrier concentrations, the recombination and generation rates, the electron and hole currents, etc. []. Once these variables have been identified according to the depth, it is easy to evaluate the carrier concentrations, electric fields, the current density-voltage characteristics (*J-V*) and the quantum efficiency (*QE*) curves, and the photovoltaic output parameters resembling the open-circuit voltage (V_{oc}), short-circuit current density. (J_{sc}), fill factor (*FF*) and the efficiency (η) [6]. These parameters describe the performance of solar cells [38,39], modeling of solar cells has the benefit that all device and material properties are well restricted as they are input parameters of the model. Therefore, trend assessment and quantified changes in *J-V* or *QE* measurements are probable.

The typical CZTSSe solar cell proposed and used for the simulation is illustrated in Figure III.11.

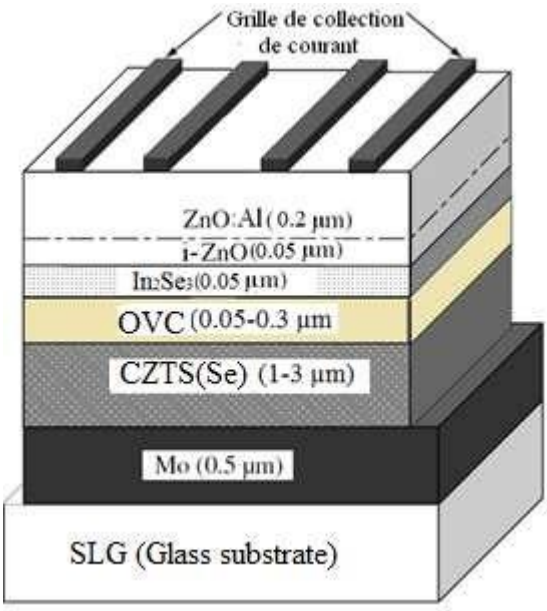

Figure III.11: Device structures of a substrate CZTSSe solar cell.

To simulate the performance of CZTSSe solar cell, the simulations need the input of device parameters, and the interface recombination velocities have been fixed as 10^7 cm/s. The light reflection of the rear and the front contacts were assumed to be 1 and 0.1, respectively. The AM 1.5D solar radiation was employed as the illumination source, corresponding to a power of 1000 W/m^2. The parameters of each semiconductor the typical cell used in the simulation were given in Table I. Reported in the literature [14,40,41].

Table 1 Input parameter values adopted for the CZTSSe solar cells in the simulations.

Parameters	**n-ZnO :Al**	**i-ZnO**	**n-In_2Se_3**	**n-OVC**	**p-CZTS**	**P^{++}CZTS**
Layer thikness : d (nm)	300	50	50	50	2000	50
Dielectric constant : ε_r	9	9	10	13.6	13.6	13.6
Effective conduction band density : Nc (cm^{-3})	$2.2x10^{18}$	$2.2x10^{18}$	$2.2x10^{18}$	$2.2x10^{18}$	$2.2x10^{18}$	$2.2x10^{18}$
Effective valence band density : Nv (cm^{-3})	$1.8x10^{19}$	$1.8x10^{19}$	$1.8x10^{19}$	$1.8x10^{19}$	$1.8x10^{19}$	$1.8x10^{19}$
Doping concentration: (Na/Nd) (cm^{-3})	$1x10^{19}$	$1x10^{14}$	$1x10^{16}$	$5x10^{15}$	$2x10^{16}$	$5x10^{17}$
Band gap : Eg (eV)	3.30	3.30	2.40	1.30	1.20	1
Electron affinity : χ (eV)	4.00	4.00	3.80	4.10	4.10	4.30
Electron mobility : μ_e ($cm^2/V.s$)	100	100	50	10	50	50
Hole mobility : μ_h ($cm^2/V.s$)	25	25	12	5	12	12
Defect density: N_{DG}/N_{AG} (cm^{-3})	$1.5x10^{14}$	$1.5x10^{14}$	$1.5x10^{17}$	$1x10^{12}$	$1x10^{12}$	$1x10^{17}$
Capture cross-section electrons: σ_e (cm^2)	$1x10^{-13}$	$1x10^{-13}$	$1x10^{-17}$	$1x10^{-13}$	$1x10^{-13}$	$1x10^{-13}$
Capture cross-section holes: σ_h (cm^2)	$1x10^{-15}$	$1x10^{-15}$	$1x10^{-12}$	$1x10^{-15}$	$1x10^{-15}$	$1x10^{-15}$

III.5 Simulation results and interpretations

The motivation of this work is to study the effect of the composition of the absorber layer based on CZTSSe compounds on the photovoltaic parameters. This study is carried out by simulations of CZTSSe -based solar cells, with a variable ratio of chalcogen elements in the absorber, with the objective of determining the optimal composition of the absorber. We show the role of the formation of the ordered Vacancy compound (OVC) layer between the buffer layer and the absorber part on the performance of the device. And the effect of (p^{++}CZTS) which serve as back surface field (BSF) between the absorber and the Mo back contact.

III.6.1 Effect of the composition of the absorber $Cu_2ZnSn(S_xSe_{1-x})_4$: x = [S]/([S]+[Se]).

In this part, we will discuss the effect of the S content x=[S]/([S]+[Se]) in the absorbent layer on the efficiency of the cell and the origin of the various losses. We will then present the results obtained. For this, we need to know the variation of the band gap energy (E_g) as a function of the composition of the $Cu_2ZnSn(S_xSe_{1-x})_4$ (CZTSSe) alloy in the structure of the solar cell. . The dependence of these parameters on x is given by the following equation [11]:

- ✓ $E_g(x) = (1-x)E_g(CZTSe) + x\,E_g(CZTS) - bx(1-x)$, (III.5)

Where $b = (0.11)$;

Figure III.12 shows the effect of the S content on the *J(V)* characteristic. Note that the more the concentration x increases, the more the photovoltaic properties are affected:

- Low Increases of the photocurrent when the S content.
- Increase of the open circuit voltage with the increase of the S content

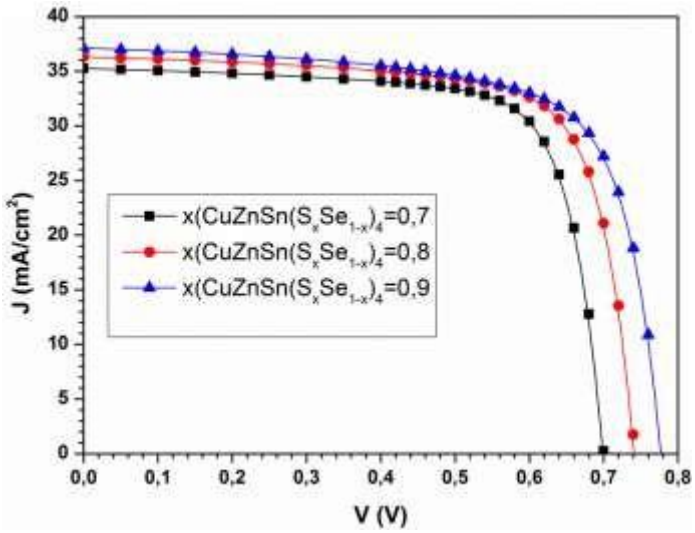

Figure III.12: *J–V* characteristics of solar cell with variable the S content of $Cu_2ZnSn(S_xSe_{1-x})_4$ absorber layer.

- The power provided by the cell increases by the addition of of sulfur (S) and decreases by the presence of selenium (Se).

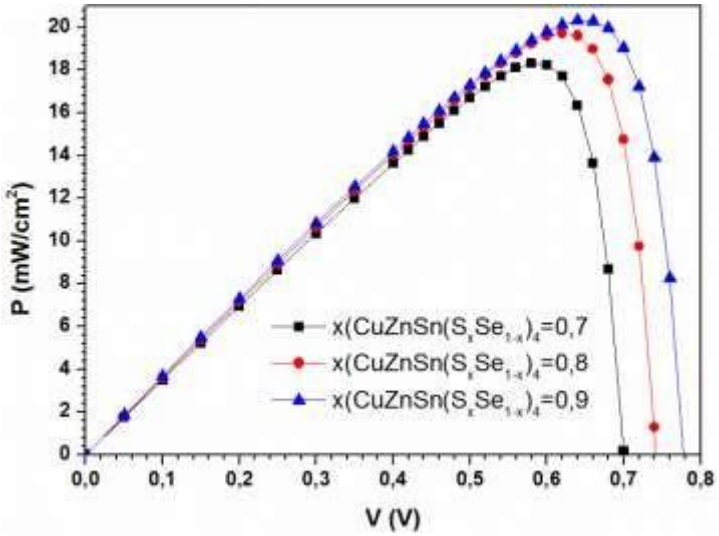

Figure III.13: *P–V* characteristics of solar cell with variable the S content of $Cu_2ZnSn(S_xSe_{1-x})_4$ absorber layer.

III.6.2 Influence of the composition of the absorber on the photovoltaic parameters:

Figure III.14 shows the positive effect introduced by the S in the $Cu_2ZnSn(S_xSe_{1-x})_4$ results in the enhancement of the photovoltage (V_{oc}) which results in an increase in the power delivered by the cell based on the ZnO/In_2Se_3/CZTS heterostructure. Due to the high mobility of copper in CZTSSe which causes vacancy and interstitial type defects, the S occupies the vacant sites of Cu and consequently reduces the recombination current.

The simulations lead to an efficiency of 16.68% (with an open circuit voltage of 0.74 V, short circuit current of 36.2 mA/cm^2 and a file factor of 70.8%) when the content of sulfur is increased linearly from the back contact towards the buffer layer. Based on these results, we propose that the band gap engineering with a variation of the rate [S]/([S]+[Se]) in the absorber is an effective way to increase the performance of CZTSSe-based solar cells without the need to change the quality of the absorber itself. Figures IV.8 indicate that the contribution of S improves the efficiency which is maximum for x = 0.7 and x=0.8 the performances are better for an optimal gap (for E_g = 1.33 -1.36 eV).

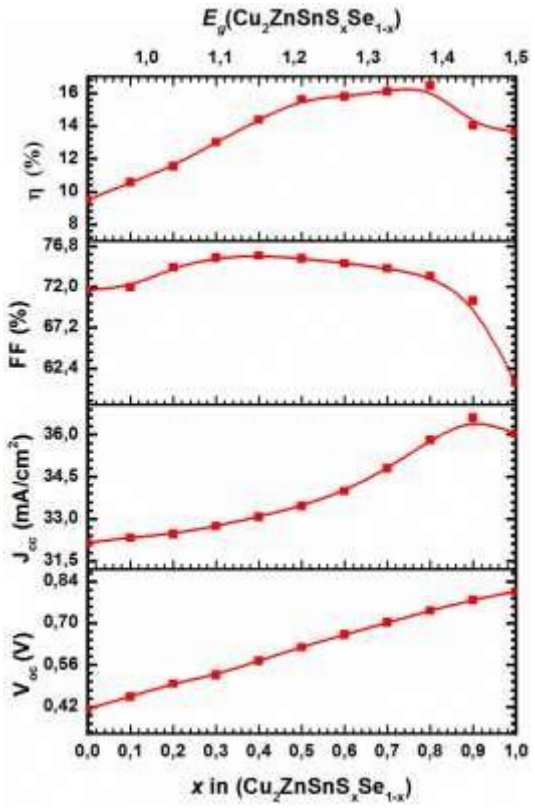

Figure III.14: *Voc*, *Jsc*, *FF* and efficiency as a function of the S content in $Cu_2ZnSn(S_xSe_{1-x})_4$ absorber layer.

IV.6.3 Effect of OVC layer:

III.6.3.1 Formation of the OVC layer at the In2Se3/CZTS interface:

The role of the CZTS surface has been widely discussed within the international community, but it is still debated today and has given rise to various interpretations as to the origin of the difference in composition between the surface and the volume of the CZTS.

The first model is that of the surface OVC layer, formed by self-reconstruction of the energetically favored surface of the system; in this model, the distance between the Fermi level and the most energetic states of the BV on the surface is larger than in the volume of the CZTS and the band gap of the OVC is about 1.4 eV, which would result in an n-type inversion at the CIGS surface with the same advantages as in the case of the CZTSSe/CdS heterojunction [26].

The induced n-type inversion would decrease when the S content level increases.

The model of Herberholz et al proposes for its origin of the surface inversion an electric field caused by positively charged donor states on the surface of the CZTS. This field would lead to an electro-migration of Cu^{+} ions within the volume, leaving a surface layer with a high concentration of negatively charged defects; combined with band curvature due to Se vacancies, it would result in a high energy barrier on the BV at the CZTS/CdS interface and prevent recombination charge carriers at the interface. Indeed, Cahen et al suggest that the surface inversion would be due to surface states such as V_{Se} selenium vacancies resulting from a surface desorption of Se; the BC would then find itself strongly curved close to the Fermi level [11,26].

In addition to the fact that it makes it possible to reduce the rate of recombinations at the interface, this inversion at the surface of the CIGS, whether caused by the diffusion of Cd or by the depletion of Cu, is also of extreme importance during the study of the defects present in the volume and on the surface of the absorber. This is particularly the case for native complex defects of type (V_{Se}-V_{Cu}) and (In_{Cu}-$2V_{Cu}$). The Lany and Zunger model predicts a non-uniform charge distribution in the absorber of these defects, which depends on the position of the Fermi level. In Figure IV.4, the distribution of complex-related defects (V_{Se}-V_{Cu}) and (In_{Cu}-$2V_{Se}$) have been separated for clarity [26].

III.6.3.2 Band diagram:

As mentioned before, it is essential to introduce, in our numerical model, a layer of OVC defects with an n-type conductivity. The main goal is to present an analysis by modeling of the impact of this existence on the characteristics of the thin film cell based on CZTS. The inversion layer which is formed experimentally by the phenomenon of inter-diffusion between the molecules of CIGS and that of In_2Se_3.

Figure III.15 represents the energy diagram of the $ZnO/In_2Se_3/Cu_2ZnSn(S_xSe_{1-x})_4$ heterostructure for x = 0.3.

According to figure III.15 the energy diagram of the simulated heterostructure presents a dipole at the top (CLIFF) at the interface of In_2Se_3- $Cu_2ZnSn(S_xSe_{1-x})_4$, in the case of CIGS and this result is generalized for the case where the content of Ga/(Ga + In) is very high. And therefore $\Delta Ec1 > 0$.

Considering for example type defects (V_{Se}-V_{Cu}), they act as positively charged donor type traps in the region where the Fermi level of the absorber is close to the BV. Close to the ZCE, when the Fermi level is about 0.2 eV above the BV, these defects form negatively charged acceptor states close to the BC

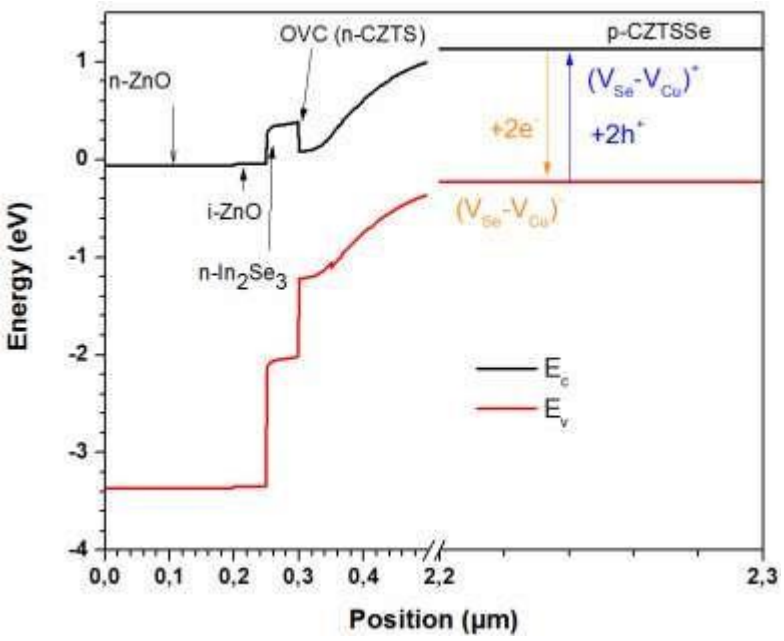

Figure III.15: band diagram of the ZnO:Al/i-ZnO/ n-In_2Se_3/p-$Cu_2ZnSn(S_xSe_{1-x})_4$heterostructure Simulate by WxAMP

The simulations made it possible to highlight the very great sensitivity of the discontinuity at the level of the conduction band. Nevertheless, this discontinuity leads to charge transport problems at the interface and is likely to degrade the performance of the cell. In order to avoid this phenomenon, it is possible to play on the thickness and the concentration of the defects of the OVC layer.

III.6.3.3 Effect of the OVC layer thickness

To introduce of the type n-OVC as the band gap energy of the Cu- poor CZTSSe layer is higher than that of CZTS bulk region with N_d =5.10^{15} cm^{-3} into the part of the absorber near to the interface p-CZTSSe/ In_2Se_3 playing a key role for achieving high-efficiency of the solar cells ZnO:Al/i-ZnO/In_2Se_3/OVC/CZTS structure. The beneficial effect obtained by the insertion of the OVC layer with 0.05 µm of thickness is illustrated in Fig. III.16, which induces the increase of the quantum efficiency $QE(\lambda)$ and this is due to the reduction of recombination at the interface CZTS/In_2Se_3. In Fig. III.17, the *J-V* characteristics of the device, with and without including the OVC, measured under AM1.5G illumination are compared. We note that the performances of the solar cells with the Cu- poor layer are superior to those of the cells without the OVC, the photo-current that is increased with the OVC is due to electron–hole pair generation.

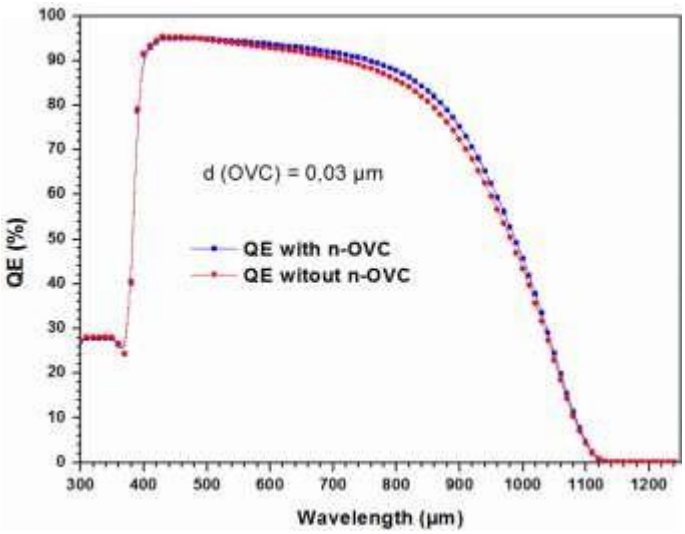

Figure III.16: Variation of the quantum efficiency of the baseline cell with and of without *n*-OVC layer

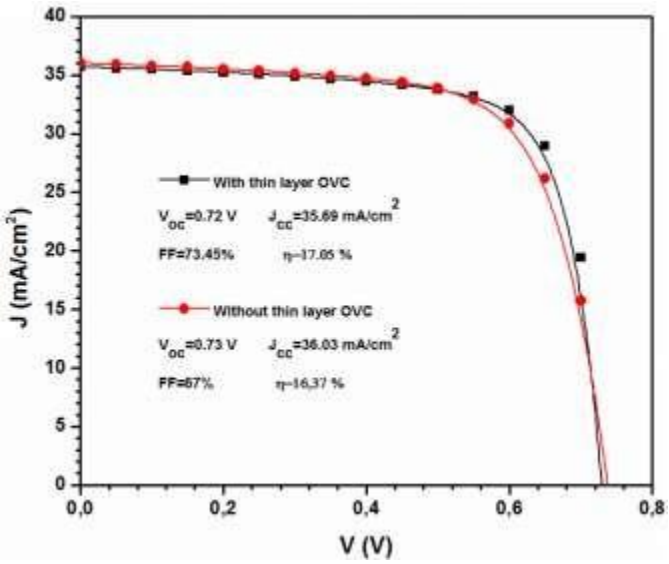

Figure III.17: Variation of *I-V* of the baseline cell with and of without *n*-OVC layer.

In Figure III.18, we show how the device performance is affected by the formation of the OVC layer in the CZTS absorber part. The performances of the respective cells for different thicknesses of n-OVC layer are shown in terms of the open circuit voltage (V_{oc}), short circuit current density (J_{sc}), fill-factor (*FF*) and efficiency (η). It is found that the values of η, *FF* and J_{sc} of the cell are increasing with the thickness of the OVC layer, which is the larger bandgap of the Cu-poor CZTS surface region in a solar cell, but start decreasing considerably from the front contact when the OVC thickness exceeds some optimal values, the decrease in *FF*, J_{sc} and η is more abrupt for larger values of OVC thickness. The best performance of the typical photovoltaic devices with the optimal OVC thickness is in the range of 40 nm–60 nm. As a result of the decrease of absorption lost in the OVC layer, a large fraction of the light is transmitted towards the absorber layer producing more amount of electron–hole pairs, which contribute to the photocurrent. Therefore, the lower thickness required for an OVC layer can lead to reduced cell material usage and lower cost of fabrication. In addition when the OVC thickness is higher than 60 nm, the cell efficiency is limited by recombination coming from different recombination mechanisms at the ODC/CZTSSe interface due the increase in series resistance. Also, the separation of excess holes generated in the OVC layer to thin p-CZTSSe region is not efficient since the optical absorption in the thick OVC layer is significant. The simulated results show that the optimal thickness of the OVC to optimize the solar cells is in the range of 40–60 nm, the best efficiency of 16.66%

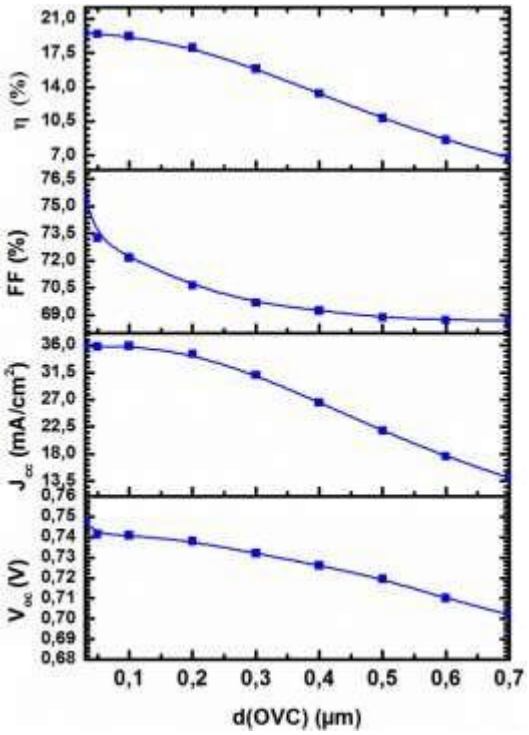

Figure III.18: Calculated dependence of solar cell parameters on OVC thickness

III.6.3.4 OVC defect density variation

As shown in Figure III.19. These defect states are acceptor-like and come from Cu vacancies (V_{Cu}), which are created by the diffusion of the Cu atoms from the absorber layer CZTSSe into the buffer layer (In_2Se_3) during growth process for the deposition of CZTSSe absorber. The Cu is the most mobile atom in the CZTSSe films and the element readily diffuses and spreads out from the middle layer to both sides, where its concentration is a function of depth. The simulation results showed that a very high performance is obtained when the defect density is in the range of 10^{12}–10^{15} cm^{-3} for both contacts. On the other hand, there was some degradation in performance for a high density due to a low *FF* resulting from the higher resistance of the OVC layer. When the defect density of the n-OVC layer is over 10^{15} cm^{-3}, J_{sc}, V_{oc}, *FF* and η decrease abruptly due to the formation of barrier against photo-generated electrons. The entire recombination increases with increasing the conduction band offset and the defect density. When the defect density is in the range of 10^{12}–10^{15} cm-3, the barrier causing recombination between majority carriers is not formed and J_{sc}, V_{oc}, *FF* and η are nearly constant. The p–n heterojunction occurs between n-OVC and p- CZTSSe, instead of being between n-In_2Se_3 and p- CZTSSe. The cell efficiency decreased when the cell was fabricated with the CZTSSe films with a high density of the OVC layer.

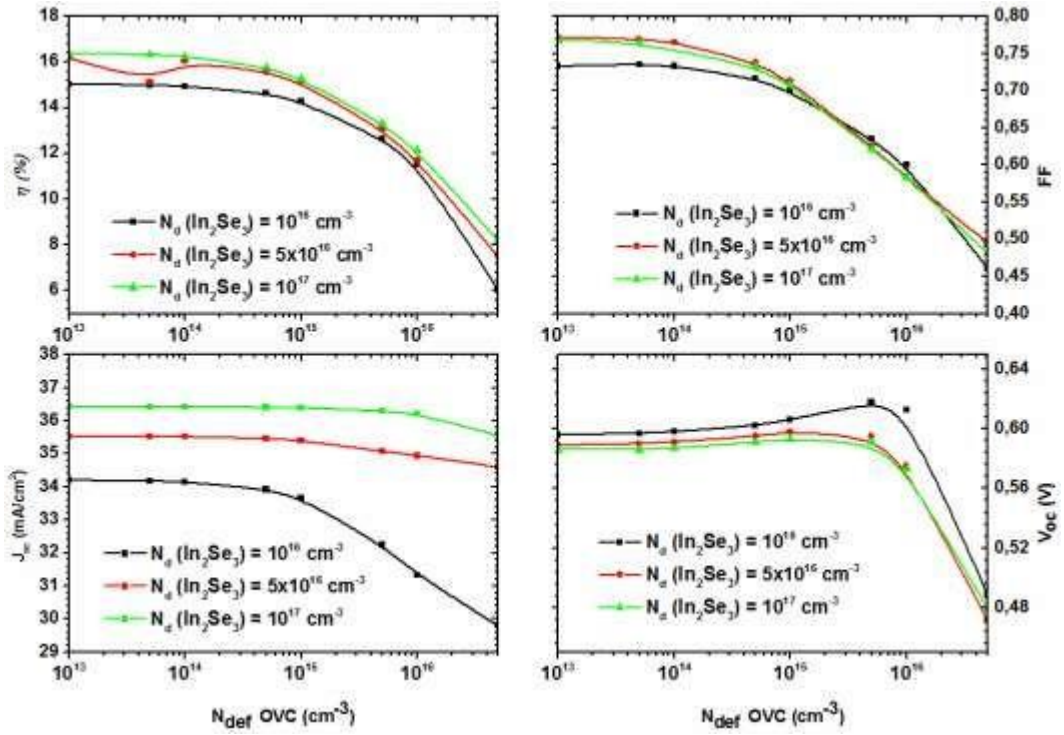

Figure III.18: The effect of the defect density of the OVC on the performance of the CZTSSe solar cell structures

III.6.4 Effect of buffer layer thickness (In_2Se_3):

The following figures represent the effect of the thickness on the photovoltaic parameters (J_{sc}, V_{oc}, *FF* and efficiency) for different thicknesses of In_2Se_3. It is clear that from figures (III.19). That the thickness of In_2Se_3 between 30-50 nm represents the optimal thickness of this buffer layer for the CZTSSe -based solar cell. The thickness of In_2Se_3 can be up to 70 nm, as the performance of the cell has a slight variation in the optimum point. The effect of the thickness of the In_2Se_3 buffer layer affects only the J_{sc} and *FF* in a remarkable way, however, the thicknesses varying between 30 and 50 nm represent the optimal thicknesses. It provides an FF of around 75 to 85%.

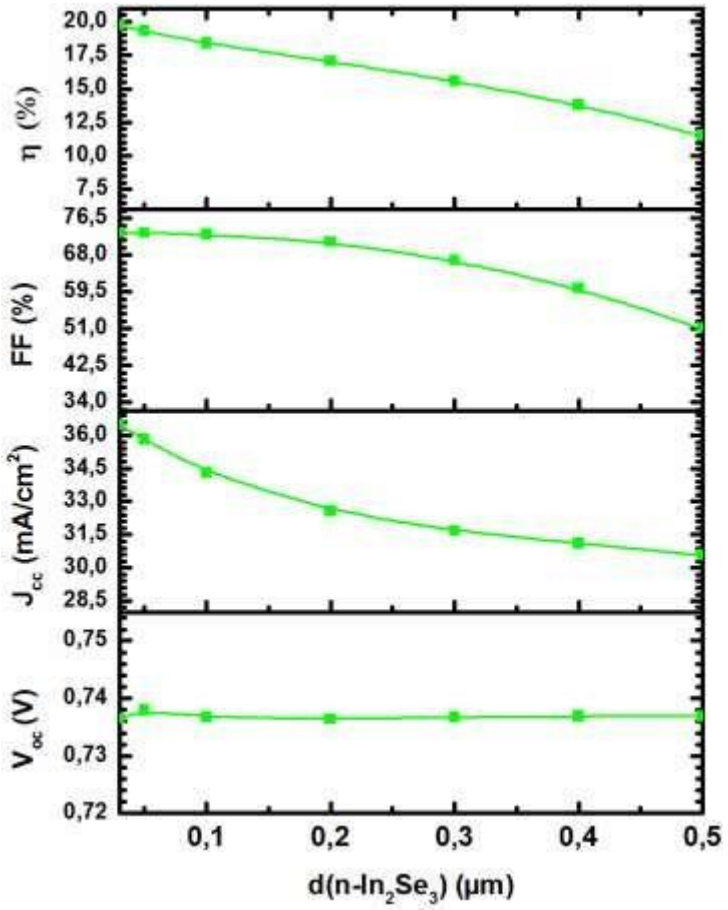

Figure III.19: Calculated dependence of solar cell parameters on buffer layer thickness

III.6.5 Back Contact Effect (BSF)

Introducing a thin layer heavily doped with p^{++} type in the part of the absorber close to the p-CZTSSe/Mo interface is a key point of the Mo/p^{++}CZTSSe/p-CZTSSe/n-In_2Se_3/i-ZnO/n-ZnO: Al/Glass cell. This layer must be as thin as possible (a few tens of nm) and must be in direct contact with Mo, for the following reasons: to increase the collection of photogenerated carriers by creating a repulsive field for minority carriers and to reduce recombination possible at the p-CZTSSe/Mo interface.

According to figure III.20 we notice that the introduction of the p^{++}CZTS layer with a thickness of 50 nm, makes it possible to establish a charge reflector at the level of the conduction band which plays a very important role, as a barrier to repel the photo-generated electrons towards the volume of the absorber. This reflector causes the formation of an electric field at the p-CZTS/(p^{++})CZTSSe interface. The device performance calculation results are shown in Figure III.20 for 30 nm thickness of the (p^{++})CZTSSE layer and for acceptor concentrations Na = 10^{18} cm^{-3}. In this case, it appears that the value of the form

factor *FF* and the open-circuit voltage V_{oc} and the short-circuit current are mainly affected. Following this variation. Indeed, the In_2Se_3/p-CZTSSe/(p^{++})CZTS/Mo:F/Glass structure makes it possible to obtain a higher form factor *FF* and consequently a better efficiency.

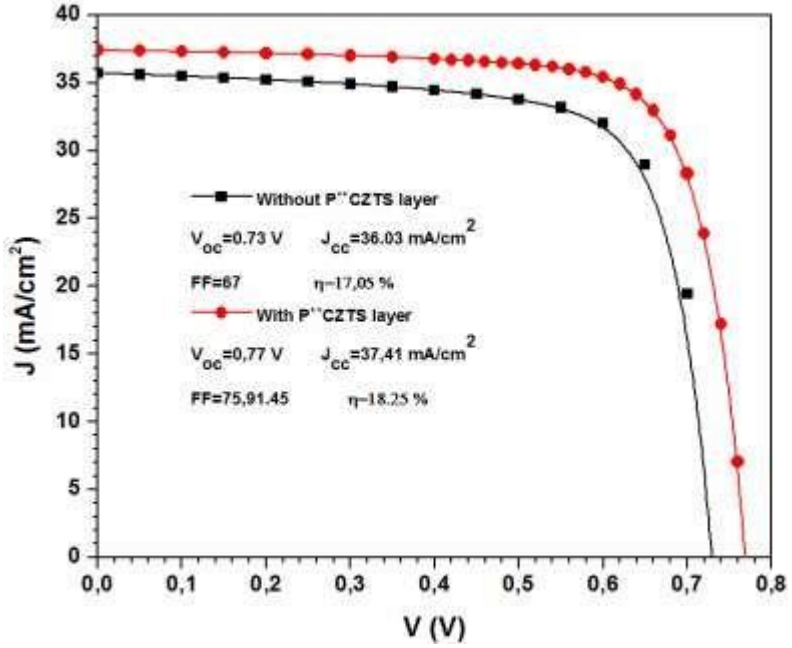

Figure III.20: *J–V* characteristics of solar cell with and without *P*$^{++}$*CZTS BSF* layer.

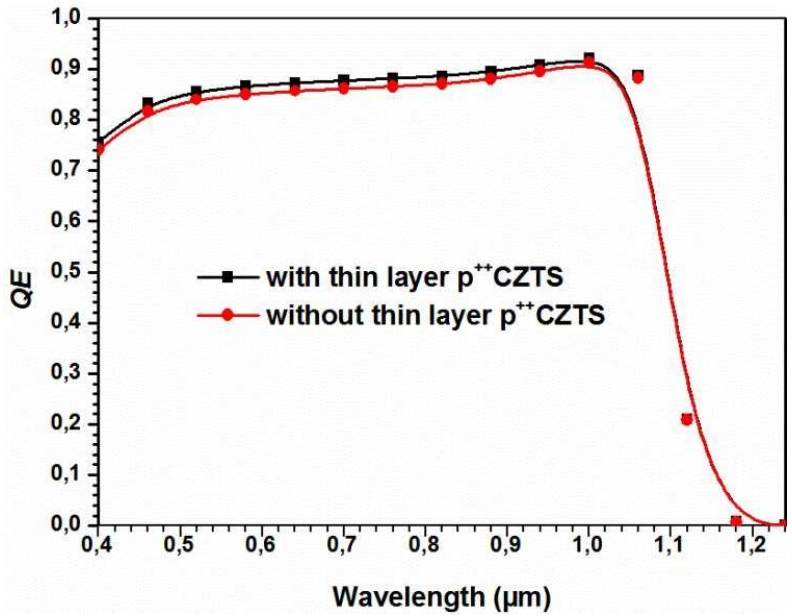

Figure III.21: Variation of the quantum efficiency of the baseline cell with and of without *P*$^{++}$*CZTS BSF* layer.

III.6.6 Influence of the rear contact function (Metal)

In order to improve the collection and so that the photo-generated carriers can be routed to the collector electrodes, it is necessary to choose a metal which has a large work function (*W*) in order to be able to improve the operation of the solar cell at the CZTS/metal interface. The carrier transport phenomenon at the CZTS/metal interface is almost identical to that at the front contact. It is based on the Schottky type junction principle. This model gives the barrier height Φ_b such as:

$$\Phi_b = W - \chi \qquad \text{(III.6)}$$

Where *W* represents the work function of the metal and χ the electronic affinity of the CZTS semiconductor.

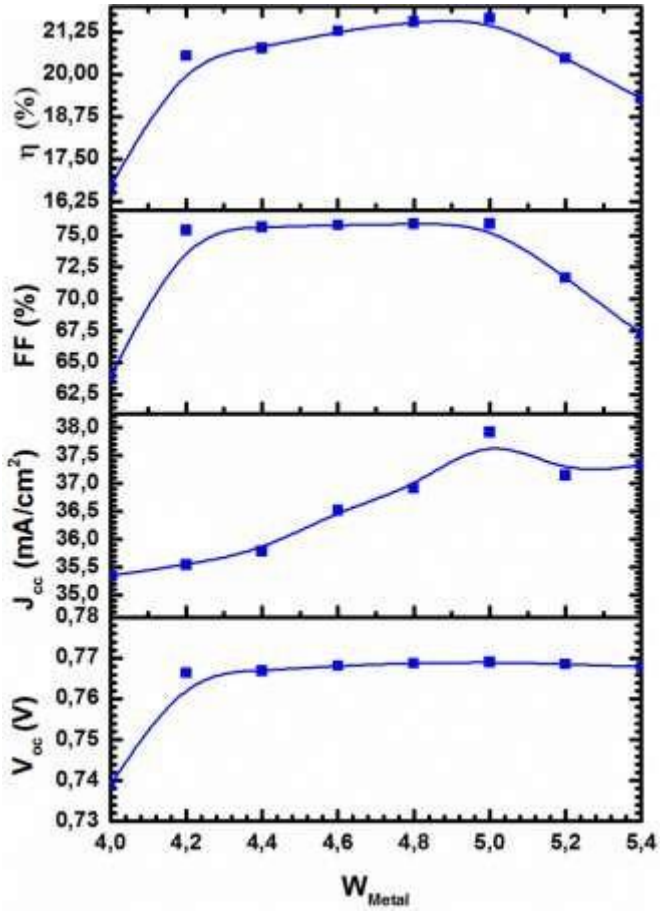

Figure III.21: Effect of the metal work function of the rear contact on the the performances of the solar cell.

In the calculations of the performances of the solar cell, when we vary the height of the barrier we find a series of curves presented in figure III.21. When the height of the barrier

increases, we reach the state of current saturation at minimum values and therefore a reversal of the curve “in English: Rollover” occurs at low applied voltage. This reversal varies over a narrow variation range of the height of the barrier. With the increase of the height of the barrier, the performances of the solar cell are affected by the reduction of the form factor FF increase of the series resistance and thus a remarkable degradation of the performances

III.7 Conclusion

In this chapter, numerical simulations were carried out by WxAMPS software to model the behavior of solar cells based on $Cu_2ZnSn(S_xSe_{1-x})_4$. A comparative study between CZTS, CZTSe, CZTSSe showed us that the absorbent layer based on CZTSSe gives best results.

We have studied the effect of the thickness, the width of the forbidden band and the concentration of the defects of the absorber layer on the photovoltaic parameters in the heterostructures of the type n-In2Se3/OVC/p-CZTSSe. Thus the effect of the metal work function of the rear contact. The results obtained show that the study of the influence of these parameters on yield leading to maximum yield. This study allowed us to optimize the electrical efficiency of the ZnO/In2Se3/CZTSSe structure. We can say that the parameters of the absorbent layer play a crucial role with respect to the performance of the studied device and in particular in the improvement of the conversion efficiency of CZTSSe-based solar cells, since they affect the electrical properties of the junction.

The results obtained show that the study of the influence of these parameters on yield leading to maximum efficiency.

General conclusion

General conclusion

The work that we carried out as part of this dissertation allowed us to study certain phenomenon which govern the operation of solar cells based on the new quaternary semiconductor material $Cu_2ZnSn(S_xSe_{1-x})_4$, (CZTS,Se) in thin layers. The latter which is currently attracting a lot of attention due to its emergence as an alternative material to conventional semiconductors.

Modeling and simulation were done by wxAMPS-1D numerical simulation software. The cell is subjected to AM1.5G illumination and an operating temperature of 300°K. The electrical current-voltage characteristics of the solar cell were calculated at each variation of parameters of the thin layers constituting the cell. From these electrical characteristics, four photovoltaic parameters can be derived that define the structure, such as: the short-circuit current density (J_{cc}), the open-circuit voltage (V_{oc}), the fill factor (FF) and the photovoltaic conversion efficiency (η).In order to optimize the performance of the latter by studying the effect of the various photovoltaic parameters, namely: the thickness of the CZT(S,Se) absorber, the concentration of these acceptors, the energy gap, the density of defects of the CZTS absorbent layer as well as the concentration of In_2Se_3/CZT(S,Se) interface defects, we will also see the impact of the buffer layer according to their thickness and the concentration of these majorities.

These characteristics are studied and analyzed under the variation of several parameters such as: Different values of the stoichiometric composition evolving with the value of the concentration ratio [S]/([S]+[Se]), surface defects and impact band gap variations on the electrical characteristics, we will also see the impact of the buffer layer according to their thickness and the concentration of these majorities, the effect of the metal work function of the rear contact.

In order to optimize the performance of the CZT(S,Se) solar cell, the simulation results obtained showed that:

- The effect of the CZTS layer has proven its effectiveness in limiting the number of simple defects caused by the vacancy of copper (a very mobile element in these compounds). These performances are deduced by optimizing the sulfur content (S) in the absorber and which is located in the interval from 0.3 to 0.5. This is due to the progressive substitution of S atoms in place of those of Zn (Sn_{Zn}) and the copper vacancies V_{Cu}. On the other hand, the drop in cell performance for $x > 0.5$ is

essentially due to the reduction in the shunt resistance R_{sh} observed on the *J-V* characteristic, and consequently a reduction in the power supplied by the cell performances are better for an optimal gap for E_g = 1.33 eV.

- The effect of the OVC layer has proven its effectiveness in limiting the number of single defects caused by the vacancy of copper (a very mobile element in these compounds). The thickness of the layer which is located in the range of 0.1 to 0.2 µm this requires having thin films. For large values of the concentration of the defects of the OVC layer (small width of the depletion zone) and large values of the density of the interface states, the performance of the solar cells is poor.
- The thickness of the In_2Se_3 layer which is located in the range of 30 to 50nm. This requires having thin films. On the other hand, the drop in cell performance for thicknesses greater than 50 nm is essentially due to the increase in the series resistance R_s observed on the *J-V* characteristic, and consequently a reduction in the power supplied by the cell. The concentration (N_d) of the In_2Se_3 layer must be very conductive, which would reduce the series resistance and allow for better efficiency.
- The role of overdoping of the thin layer p^{++}CZTS/Mo side and its effect on the collection of photo-generated carriers. The effect of the potential barrier of the rear contact of the solar cell in order to improve the collection of the photo-generated carriers.

Several perspectives can be put forward at the end of this study, such as: The possibility of developing multi-junction solar cells to achieve better conversion efficiencies. This is certainly an avenue for future research.

Bibliography

[1] H. Katagiri, K. Jimbo, S. Yamada, T. Kamimura, W.S. Maw, T. Fukano, T. Ito,T. Motohiro, Solar cell without environmental pollution by using CZTS thin films, Proceedings of Photovoltaic Energy Conversion Conference, 3 (2003).

[2] M. Y. Valakh, V. M. Dzhagan, I. S. Babichuk, X. Fontane, A. Perez-Rodriquez, S. Schorr, Optically induced structyral transformation in disordred kesterite $Cu_2ZnSn(S_xSe_{1-x})_4$, JETP Letters 98 (2013), pp. 255-258

[3] A. Lafond, L. Choubrac, C. Guillot-Deudon, P. Deniard, S. Jobic, Crystal Structures of Photovoltaic Chalcogenides, an Intricate Puzzle to Solve: the Cases of CIGSe and CZTS Materials, Journal of Inorganic and General Chemistry, 638 (2012), pp. 2571-2577.

[4] V. Chawla, A study of CZTS thin films for solar cell Applications , thesis for the degree of Doctor of philosophy, Department of materials science and engineering, Stanford university, December 2011.

[5] W. A. Hermann, Quantifying global exergy resources, Energy, 31,12 (2006), pp. 1685 – 1702,.

[6] A. Luque and S. Hegedus, Handbook of Photovoltaic Science and Engineering. Wiley, 2nd ed., mar (2011).

[7] W. Shockley and H. J. Queisser, Detailed balance limit of efficiency of p-n junction solar cells, Journal of Applied Physics, vol. 32, (1961) pp. 510–519.

[8] A. Walsh, S. Chen, S.-H Wei, X.-G. Gong, Kesterite Thin-Film Solar Cells: Advances in Materials Modelling of Cu_2ZnSnS_4 , Advanced Energy Materials, 2 (2012), pp. 400-409.

[9] C. Persson, Electronic and optical properties of Cu2ZnSnS4 and $Cu_2ZnSnSe_4$, Journal of Applied Physics, vol. 107, (2010), pp. 053710–053710–8.

[10] M. A. Green, K. Emery, Y. Hishikawa, and W.Warta, "Solar cell efficiency tables (version 37)," Progress in Photovoltaics, vol. 19, no. 1, (2011), pp. 84–92.

[11] Giovanni Altamura. Development of CZTSSe thin films based solar cells". Material chemistry. Université Joseph-Fourier - Grenoble I, 2014

[12] P. Jackson, D. Hariskos, and E. Lotter, "New world record efficiency for $Cu(In,Ga)Se_2$ thin film solar cells beyond 20%," Progress in Photovoltaics, vol. 19, no. 7, (2011), pp. 894–897.

[13] S. M. Sze, K. K. NG, Physics of semiconductor devices, Wiley (2007).

[14] S. Harel, C. Guillot-Deudon, L. Choubrac, J. Hamon, A. Lafond, Surface composition deviation of Cu_2ZnSnS_4 derivative powdered samples, Applied Surface Science, 303 (2014), pp. 107-110.

[15] T. Maeda, S. Nakamura, T. Wada, 04DP07First Principles Calculations of Defect Formation in In-Free Photovoltaic Semiconductors Cu_2ZnSnS_4 and $Cu_2ZnSnSe_4$, Japanese Journal of Applied Physics, 50 (2011),

[16] P.A. Fernandes, P.M.P. Salomé, A. F. da Cunha, Study of polycrystalline Cu_2ZnSnS_4 films by Raman scattering, Journal of Alloys and Compounds 509 (2011), pp. 7600.

[17] M Ravindiran, C Praveenkumar, Status review and the future prospects of CZTS based solar cell–A novel approach on the device structure and material modeling for CZTS based photovoltaic device Renewable and Sustainable Energy Reviews Volume 94 **(**2018**),** pp. 317-329

[18] W. Ki, H. W. Hillhouse, Earth-abundant element photovoltaics directly from soluble precursors with high yield using a non-toxic solvent, Adv. Energy Mater., 1 (2011), pp. 732–735.

[19] S. Chen, X. G. Gong, Electronic structure and stability of quaternary chalcogenide semiconductors derived from cation cross-substitution of II-VI and I-III-VI_2 compounds, Physical review B 79 (2009), pp. 165211.

[20] S. Chen, A. Walsh, J. Yang, X. G. Gong, L. Sun, P. X. Yang, J. H. Chu, S. H. Wei, Compositional dependence of structural and electronic properties of $Cu_2ZnSn(S,Se)_4$ alloys for thin film solar cells, Physical review B B 83 (2011), pp. 125201.

[21] M. Y. Valakh, V. M. Dzhagan, I. S. Babichuk, X. Fontane, A. Perez-Rodriquez, S. Schorr, JETP Letters 98 (2013), pp. 255-258

[22] T. K. Todorov, K. B. Reuter, and D. B. Mitzi, "High-efficiency solar cell with earth-abundant liquid-processed absorber," Advanced Materials, vol. 22, (2010), pp. E156–E159.

[23] H. Katagiri, Enhanced Conversion Efficiencies of Cu_2ZnSnS_4 Based Thin Film Solar Cells by Using Preferential Etching Technique, Appl. Phys. Express, 041201 (2008).

[24] C. Li, M. Cao, J. Huang, Y. Sun, L.J. Wang, Y. Shen, Effects of S and Se contents on the physical and photovoltaic properties of $Cu_2ZnSn(S_xSe_{1-x})_4$ nanoparticles, Journal of Alloys and Compounds 616, (2014), pp. 542–549.

[25] A. Fernandes, P. M. P. Salomé, A. F. Sartori, J. Malaquias, A. F. Da Cunha, B.Schubert, G. M. Ribeiro, Effects of sulphurization time on Cu_2ZnSnS_4 absorbers and thin films solar cells obtained from metallic precursors,Solar Energy Materials and Solar Cells, 115 (2013), pp. 157-165

[26] K. Biswas, S. Lany, and A. Zunger, The electronic consequences of multivalent elements in inorganic solar absorbers: Multivalency of Sn in Cu_2ZnSnS_4 ,Appl. Phys. Lett.96 (2010), pp. 201902.

[27] W. Wang, M. T. Winkler, O. Gunawan, T. Gokmen, T. K. Todorov, Y. Zhu, D. B. Mitzi, Device Characteristics of CZTSSe Thin-Film Solar Cells with 12.6% Efficiency ,Adv. Mater. Vol. 4, 7, (2014), pp.1301465

[28] A. Redinger , D. M. Berg, P. J. Dale, S. Siebentritt, The Consequences of Kesterite Equilibria for Efficient Solar Cells, J. Am. Chem. Soc., 133 (2011), pp. 3320–3323

[29} A.V. Moholkar, S.S. Shinde, G.L. Agawane, S.H. Jo, K.Y. Rajpure, P.S. Patil, C.H. Bhosale, J.H. Kim, 151Studies of compositional dependent CZTS thin film solar cells by pulsed laser deposition technique: An attempt to improve the efficiency , Journal of Alloys and Compounds, 544 (2012), pp. 145-151.

[30] H. Xin, H.W. Hillhouse, 8.3% Efficient copper zinc tin sulfoselenide solar cells processed from environmentally benign solvent, in: Proceedings of the 39th IEEE Photovoltaic Specialists Conference, (2013).

[31] S. Ahmed, K.B. Reuter, O. Gunawan, L. Guo, L.T. Romankiw, H. Deligianni, A high efficiency electrodeposited Cu_2ZnSnS_4 solar cell, Advanced Energy Materials 2 (2012), pp. 253–259.

[32] I. Repins, M. A. Contreras, B. Egaas, C. DeHart, J. Scharf, C. L. Perkins, B. To, and R. Noufi, 19.9%-efficient ZnO/CdS/$CuInGaSe_2$ solar cell with 81.2% fill factor, Progress in Photovoltaics: Research and Applications, vol. 16, no. 3, (V), pp. 235–239.

[33] M. A. Contreras, M. J. Romero, B. To, F. Hasoon, R. Noufi, S. Ward, and K. Ramanathan, Optimization of CBD CdS process in high-efficiency Cu(In,Ga)Se_2-based solar cells, Thin Solid Films, vol. 403-404, (2002), pp. 204–211.

[34] Yiming Liu , Yun Sun [a], Angus Rockett, A new simulation software of solar cells—wxAMPS, Solar Energy Materials and Solar Cells 98, (2012), pp 124-128.

[35] Yanping Wang , Jiao Wang , Haoran Li , Aimei Zhao , Bing Li , Jinlian Bi wxAMPS theoretical study of the bandgap structure of CZTS thin film to improve the device performance, Optoelectronics Letters 17, (2021), pp. 475–481

[36] Y. Liu, Y. Sun, and A. Rockett, Batch simulation of solar cells by using Matlab and wxAMPS, 38th IEEE in Photovoltaic Specialists Conference (PVSC), (2012).

[37] John Arch, Joe Cuiffi, Jingya Hou, William Howland, Peter McElheny, Anthony Moquin, Michael Rogosky, Thi Tran, Hong Zhu, and Francisco Rubinelli; AMPS Manual. The Center for Nanotechnology Education and Utilization, The Pennsylvania State University, University Park, PA 16802, (1994).

[38] Y. Liu, D. Heinzel, and A. Rockett, A Revised Version of the AMPS Simulation Code, in Photovoltaic Specialists Conference (PVSC), 2010 35th IEEE, (2010), pp. 001943-001947.

[39] Dr. Yiming Liu, Brief Introduction of wxAMPS, 37th IEEE in Photovoltaic Specialists Conference (PVSC), (2011).

[40] Rabin Paul, S. Vallisree, T. R. Lenka, Modeling and Simulation of CZTS Thin-Film Solar Cell for Efficiency Enhancemen, Journal of Electronic Materials, 51, (2022), pp. 2228–2235

[41] B. Yassine, B. Tahar, G. Fathi, Modeling and simulation of CZTS based solar cells with ZnS buffer layer and ZnO:F as a window layer using SCAPS-1D, Chalcogenide Letters 19, (2022), pp. 503-511

Résumé :

Dans ce travail nous avons étudié les caractéristiques électriques d'une cellule solaire à base de $Cu_2ZnSn(S_xSe_{1-x})_4$. Pour optimiser la cellule solaire, nous avons procédé à la simulation de la structure de type: Al/ZnO/i-ZnO/In_2Se_3/CZTSSe/Mo/Verre en couches minces à l'aide d'un logiciel wxAMPS-1D, afin de déterminer les conditions optimale des couches minces de CZTSSe, leurs propriétés physiques, optique et l'effet de la variation du rapport [S]/([S]+[Se]) Nous montrons le rôle de la formation de la couche de composés lacunaires ordonnés (OVC) entre la couche tampon et la partie absorbante sur les performances du dispositif étudié. Nous montrons le rôle de la formation de la couche de composés lacunaires ordonnés (OVC) entre la couche tampon et la partie absorbante sur les performances du dispositif étudié.

Les résultats de la simulation obtenus ont montré que : Il est important de contrôler et même de limiter la concentration des défauts dans la couche absorbante si on veut produire des cellules CZTSSe efficaces. l'apport du Soufre dans $Cu_2ZnSn(S_xSe_{1-x})_4$ améliore le rendement qui est maximale pour x varie de 0.6 à 0.8 et les performances sont meilleures *(η=16.6%)* pour un gap optimal (pour E_g compris entre 1.3 et 1.38 eV) .Les résultats obtenus montrent que cette couche OVC est importante.Ainsi les performances des cellules solaires sont optimales pour des valeurs de la fonction de travail du métal du contact arrière *W* (5.3 à 5.6 eV), afin d'améliorer le collecte des porteurs photo-générés.

Mots clés : Simulation numérique, Cellule solaire, $Cu_2ZnSn(S_xSe_{1-x})_4$, OVC, rendement, wxAMPS

Abstract:

In this work we studied the electrical characteristics of a solar cell based on $Cu_2ZnSn(S_xSe_{1-x})_4$ To optimize the solar cell, we simulated the structure of the type: Al/ZnO /i-ZnO/In_2Se_3/CZTSSe/Mo / Thin film glass using wxAMPS-1D software, in order to determine the optimal conditions of CZTSSe thin films, their physical and optical properties and the effect of varying the ratio [S]/([S]+[Se]). We show the role of the formation of the ordered vacancy compound (OVC) layer between the buffer layer and the absorber part on the performance of the devic studied.

The simulation results obtained showed that: It is important to control and even limit the concentration of defects in the absorbent layer if one wants to produce efficient CZTSSe cells. The contribution of Sulfur in $Cu_2ZnSn(S_xSe_{1-x})_4$ improves the efficiency*(η=16.6%)* which is maximum for x varies from 0.6 to 0.8 are better for an optimal gap (for E_g between 1.3 and 1.38 eV), and the obtained results show that this defect OVC layer is important in the photovoltaic performance of CZTSSe device performances. Thus the performance of solar cells is optimal for values of the metal working function of the rear contact W (5.3 to 5.6 eV), in order to improve the collection of photo-generated carriers.

Keywords: Numerical simulation, Solar cell, $Cu_2ZnSn(S_xSe_{1-x})_4$, OVC, efficiency; wxAMPS-1D.

ملخص :

في هذا العمل درسنا الخصائص الكهربائية للخلية الشمسية على أساس $Cu_2ZnSn(S_xSe_{1-x})_4$. لتحسين الخلية الشمسية ، قمنا بمحاكاة خلية من النوع: الزجاج/Al/ZnO/ i-ZnO/ In2Se3/CZTSSe/Mo باستخدام برنامج wxAMPS-1D ، من أجل تحديد الظروف المثلى للأغشية الرقيقة CZTSSe ، الخواص الفيزيائية والبصرية وتأثير تباين النسبة ([S]/([S] + [Se]) . نركز على دور تشكيل الطبقة المركبة المجوفة (OVC) بين الحشوة والجزء الممتص على أداء الخلية الشمسية المدروسة.

أظهرت نتائج المحاكاة التي تم الحصول عليها ما يلي: من المهم أيضًا التحكم في تركيز العيوب في الطبقة الماصة وحتى الحد منها إذا كان المرء يريد إنتاج خلايا CZTSSe فعالة. تعمل مساهمة الكبريت في $Cu_2ZnSn(S_xSe_{1-x})_4$على تحسين المردود *(η=16.09%)* الذي يبلغ الحد الأقصى لـ x يتغير من0.6 إلى 0.8 ويكون الأداء أفضل للفجوة المثلى (على سبيل المثال بين 1.3 و 1.38 الكترون فولت). وتظهر النتائج التي تم الحصول عليها أن طبقة OVC هذه مهمة في الأداء الخلايا الشمسية وهي الأمثل لقيم وظيفة عمل المعادن للتلامس الخلفي W(5.3 إلى 5.6 الكترون فولت) ، من أجل تحسين مجموعة الناقلين المولدة بالكهروضوئية.

الكلمات المفتاحية: محاكاة عددية ، خلية شمسية ، $Cu_2ZnSn(S_xSe_{1-x})_4$ ، OVC ، المردود, wxAMPS-1D.